NOTICE

The quality of this microform is heavily dependent upon the quality of the original thesis submitted for microfilming. Every effort has been made to ensure the highest quality of reproduction possible.

If pages are missing, contact the university which granted the degree.

Some pages may have indistinct print especially if the original pages were typed with a poor typewriter ribbon or if the university sent us an inferior photocopy.

Reproduction in full or in part of this microform is governed by the Canadian Copyright Act, R.S.C. 1970, c. C-30, and subsequent amendments.

AVIS

La qualité de cette microforme dépend grandement de la qualité de la thèse soumise au microfilmage. Nous avons tout fait pour assurer une qualité supérieure de reproduction.

S'il manque des pages, veuillez communiquer avec l'université qui a conféré le grade.

La qualité d'impression de certaines pages peut laisser à désirer, surtout si les pages originales ont été dactylographiées à l'aide d'un ruban usé ou si l'université nous a fait parvenir une photocopie de qualité inférieure.

La reproduction, même partielle, de cette microforme est soumise à la Loi canadienne sur le droit d'auteur, SRC 1970, c. C-30, et ses amendements subséquents.

The Study of Differential 8-PSK Trellis-Coded Modulation in Indoor Wireless Communications Through Computer Simulation

by

Richard V. Paiement, B.A.Sc.

A thesis submitted to the
School of Graduate Studies and Research
in partial fulfillment of the requirements
for the degree

Master of Applied Sciences

Ottawa-Carleton Institute for Electrical Engineering
Department of Electrical Engineering
Faculty of Engineering
University of Ottawa

ISBN 0-315-75084-7

Canada

UNIVERSITÉ D'OTTAWA
UNIVERSITY OF OTTAWA

Abstract

This thesis work studies the use of 4- and 8-state trellis-coded modulation with phase-shift keying and non-coherent, differential signaling for digital indoor wireless communications, at an operating frequency of 1.5 GHz and a transmission rate of 10 Mbits/s. Many other modulation schemes have been considered for the indoor wireless channel in other studies, and trellis-coded modulation has been considered for the satellite and mobile channel. This study presents new BER performance results, obtained through computer simulations, that suggest a performance gain with TCM relative to DQPSK, for certain ranges of SNR and rms delay spread. Equalization is also considered, and it is shown that it can provide considerable performance gain.

Acknowledgements

Many people contributed to my sanity over the two year period while I undertook the research work for this thesis.

I thank my parents and family for support, encouragement and understanding during my whole University sojourn.

I would like to thank my thesis supervisor, Dr. Jean-Yves Chouinard, for allowing me great freedom and making himself available beyond expectation.

I also wish to thank Drs Abbas Yongaçoğlu, Peter J. McLane and Samy A. Mahmoud for their useful suggestions, and Dr. William McGee for financial support in the initial stage of my research.

I am grateful for the many discussions, topical or not, with fellow graduate students and support staff in Electrical Engineering. I am also indebted to the department support staff, including William Keays and Steve Symons, computer system operators/analysts, for keeping the system running and putting up with my unending requests, and Suzanne St-Michel, administrative officer, for making the administrative side of things more bearable.

I would also like to acknowledge the Telecommunications Research Institute of Ontario (TRIO) and the Natural Sciences and Engineering Research Council of Canada (NSERC) for funding which made this work possible.

Contents

List of Figures

List of Tables

Acronyms

AWGN	additive white Gaussian noise
BER	bit error rate
BPSK	binary phase shift keying
DEPSK	differentially encoded phase shift keying (coherent signaling)
DFE	decision-feedback equalizer
DPSK	differentially detected phase shift keying (non-coherent signaling)
DQPSK	differentially detected quadrature phase shift keying
DS-SS	direct sequence spread spectrum
ECL	minimum effective code length
ED	Euclidean distance
FSK	frequency shift keying
ISI	intersymbol interference
IW	indoor wireless
LAN	local area network
LOS	line of sight
M-PSK	M-ary phase shift keying
MLSE	maximum likelihood sequence estimation
MSE	mean square error (equalizer performance criterion)
MSK	minimum shift keying

OQPSK	offset quadrature phase shift keying
PD	product distance
PSK	phase shift keying
QAM	quadrature amplitude modulation
QPSK	quadrature phase shift keying (4-PSK)
RMS	root mean square
SNR	signal to noise ratio
SS	spread spectrum
TCM	trellis-coded modulation
TDMA	time division multiple access
VA	Viterbi algorithm

Nomenclature

$\mathbf{C}$	equalizer tap weight coefficients vector composed of elements $\{c_j\}$
$d(x, y)$	Euclidean distance metric between x and y
d_{free}	free Euclidean distance
d_p	minimum product distance
D	decoding depth
E_b	received signal energy per bit
E_s	received signal energy per symbol
E_{PSK}	transmitted energy for a PSK system
f_c	carrier (or operating) frequency
f_D	Doppler frequency
$\{f_n\}$	tap weight coefficients of the discrete-time channel model
$G(1\text{ m})$	multipath power gain with antenna separation $r = 1$ m
$\overline{G(r)}$	average multipath power gain
G	coding gain
G_t	transmitting antenna gain
G_r	receiving antenna gain
$\mathbf{G_k}$	gradient vector used in steepest descent algorithm
$h(t)$	complex low-pass impulse response of the indoor wireless channel
I_k	symbol at the k^{th} signaling interval

$\hat{I}_k$	estimate of the symbol
$\tilde{I}_k$	detector output estimate of the symbol
J	length in symbols of transmitted sequence
K, K_1, K_2	specifies the number of taps in the equalizer:
	$(2K + 1)$ taps in the transversal equalizer;
	$(K_1 + 1)$ feed-forward taps and K_2 feedback
	taps in the decision-feedback equalizer
$(L + 1)$	number of taps in the discrete-time channel model
m	number of bits at the input to the TCM convolutional encoder
M	number of signals from the set that can be transmitted
N	diversity order
$N(d_{free})$	number of error sequence with distance d_{free}
N_o	noise power spectral density
P_b	probability of bit error
P_E	probability of event error
P_{rec}	power received at 1 metre
P_{trans}	power transmitted
$P(\tau_{kl})$	power delay profile of the impulse response
R_c	encoder rate
R_b	data bit rate
R_s	data symbol rate
r	antenna separation (in metres)
S	column vector to solve the equalizer tap coefficients
T_b	bit period
T_s	symbol period

T_l	propagation delay of cluster (in seconds)
$\{v_k\}$	signal sequence at the input to the equalizer
V	velocity of the mobile unit (in metres per second)
$\{x_l\}$	sampled auto-correlation of the channel impulse response
α	distance-power law exponent
β_k, β_{kl}	real positive gain of ray in impulse response
$\overline{\beta_{kl}^2} = \overline{\beta^2(k,l)}$	average power gain of the k^{th} ray in the l^{th} cluster
δ	effective length of an error path
δ_H	effective code length
Δ_n	minimum distance between signals (or symbols) in the n^{th} subset
$\underline{\Delta_p}$	product distance
Δ_ϕ	phase offset
∂	step size in the algorithm for adaptive equalization
γ	power-delay time constant of the rays
Γ	power-delay time constant of the clusters
$\vec{\Gamma}$	covariance matrix to solve the equalizer tap coefficients
λ_c	radio frequency carrier wavelength
λ	mean arrival rate of the rays
λ_{max}	largest eigenvalue of the covariance matrix $\vec{\Gamma}$
Λ	mean arrival rate of the clusters
ν	code constraint length
$\rho(\tau)$	delay spread function
σ_T	rms delay spread; square root of the impulse response power delay profile's second moment
$\overline{\sigma_T}$	averaged rms delay spread

σ_N	normalized rms delay spread
τ_k, τ_{kl}	propagation delay of ray (in seconds)
$\overline{\tau}$	average delay of the impulse response power delay profile
θ_k, θ_{kl}	phase shift of ray (in radians)

Chapter 1

Introduction

There is presently considerable interest within the digital communication community about universal portable radio communications [1, 2, 3], where various systems are merged, including cellular telephones networks, mobile satellite systems, and newer portable communication systems. Only in the last few years has radio communication been widely considered for indoor needs [4, 5]. The services to be covered by such wireless indoor communication systems include voice and data for multiple users, so a wide-band network approach is preferred. For it to be considered as an alternative to its wire counterpart, it must be able to operate at considerable data rates, on the order of a few Mbits/s, for example 10 Mbits/s to compete with Ethernet.

Such an indoor wireless network, where the base station and the remote stations are either stationary or slowly moving, avoids the wiring and interface problems of existing wire-line networks, but other complications exist due to the radio channel. Indoor radio propagation is afflicted by fading and dispersion, and the channel is continuously changing. It is found that these impairments limit the data rate severely; for example, with a BPSK system, the bit rate R_b is limited to values below 1 Mbit/s [6]. Therefore, techniques such as diversity, equalization and coding are required to reduce the effect of these impairments on the transmission, and permit higher data

rates. Any design should seriously consider bandwidth efficient techniques, given the ever increasing demand for more radio services.

Studies of indoor wireless communication systems have considered various modulation schemes, such as BPSK [6, 7], QPSK [8, 9, 10, 11], frequency hopped FSK [12, 13], 4-QAM [14, 15] and direct sequence spread spectrum [16, 17, 18].

This study proposes trellis-coded modulation (TCM) with phase-shift keying (PSK) and non-coherent (differential) signaling for use with an indoor wireless network. TCM has previously been studied for satellite communication channels [19, 20, 21, 22, 23] and mobile channels, but to the author's knowledge, it has never been applied to the indoor wireless channel. Equalization is also considered to get an idea of the performance gains possible with different configurations. Using a statistical model of the indoor radio channel, the probability of error for these techniques are reported, as obtained through computer simulations.

1.1 Thesis Organization

It is necessary to describe the indoor wireless propagation environment to be able to understand how it affects transmitted signals. This is done in Chapter 2, where fading and dispersion impairments of the channel are explained, and a channel model, as developed in [24], is presented. It is shown that the rms delay spread measure σ_T is a useful parameter to characterize the channel. Interleaving and diversity are considered to reduce the effect of the channel impairments.

Coding and equalization are presented in Chapter 3 as channel impairment countermeasures. Coding is suggested with bandwidth efficiency in mind, so TCM is presented, as developed for both the Gaussian and the fading channels. An overview of the Viterbi algorithm, used to decode trellis-coded signals, is also presented. Performance of 4- and

8-state 8-PSK TCM is presented as given in the literature for the Gaussian channel. Equalization is presented in its linear (transversal equalizer) and non-linear (decision-feedback equalizer) forms. Non-coherent signaling considerations relating to TCM and adaptive DFE are mentioned.

The communication system components, as used in the computer simulations, are presented in Chapter 4, along with preliminary simulation results using the Gaussian channel for comparison with theory and other published simulation results. The situation considered is for a system operating with a carrier frequency $f_c = 1.5$ GHz and a data rate $R_b = 10$ Mbits/s. The channel as used in the simulations is described in detail, and its rms delay spread statistics are given. QPSK, used as a BER performance reference, and 8-PSK TCM are described. Linear equalization is also described, as are the various methods used to obtain the equalizer's tap weight coefficients. The software platform used to develop the simulation tools and various system components is presented, as is the measure used in this work to obtain a typical representative value from the simulation results, namely the geometric mean.

The simulated performance results, for QPSK and 4- and 8-state TCM, and some specific cases with a linear equalizer, are presented and analysed in Chapter 5, and a comparison is made with available literature results.

The thesis is wrapped up with final conclusions, and some recommendations about possible future research on related topics are given.

Chapter 2

Indoor Wireless Channel

In order to analyze the performance of a system used in the indoor wireless (IW) channel, a model must be available to properly describe the channel. This model must account for all impairments, such as fading and dispersion, that can affect the received waveform. These impairments are first described, and their causes explained in Section 2.1. A discrete statistical model is presented in Section 2.2 for the IW channel. Section 2.3 suggests characterizing the channel using the rms delay spread of the impulse response. Finally, Section 2.4 considers methods to reduce the effect of channel impairments on the signal.

2.1 Fading and Dispersion

The IW channel is considered to be a harsh environment for wide-band/high-speed radio transmission because of numerous signal scatterers such as walls, ceilings, doors, furniture and people, some of which may not be fixed.

These scatterers may cause shadow fading due to blockage and attenuation from interfering scatterers, and frequency-selective fading and multipath distortion due to random fluctuations in the sum of the reflected multipath phases. These effects vary dynamically with time as the environment slowly changes, and can be analyzed statis-

tically.

In such a multipath environment, paths of different lengths cause spreading in time of the transmitted signal waveform. This spreading, or dispersion, produces intersymbol interference (ISI) which limits the maximum data rate of the channel. Also, with increasing signal to noise ratio (SNR), a floor in bit error rate (BER) performance is approached, beyond which there is no further BER reduction because the ISI increases proportionally to the signal power level.

In addition, the IW channel suffers from received signal power variations caused by frequency-selective and shadow fading. This is observed as slow fading, where a deep fade can last for long periods of time (on the order of a few seconds to a few minutes).

Another inherent cause of deep fading in a portable environment such as the IW channel is random antenna orientation, which creates polarization misalignment of the randomly oriented mobile antenna [25].

These fading and dispersion impairments in the frequency-selective channel increase the probability of signal outage, cause irreducible BER performance, and limit the maximum data rate. If the IW channel, and thus these disturbances, can be properly modeled, it is then easier to see how they affect performance and how they can be handled to reduce their effect.

2.2 Indoor Wireless Channel Model

For a transmitted waveform $x(t)$ and the corresponding received waveform $y(t)$, a channel can be characterized by the impulse response $h(t)$, where:

$$y(t) = f(x(t), h(t)) \tag{2.1}$$

Because of scatterers, the received waveform contains attenuated and time delayed

versions of the transmitted waveform. Using this representation, the multipath channel is described simply by using a discrete model with a complex low pass impulse response [26, pp.703-713]:

$$h(t) = \sum_k \beta_k(t) e^{j\theta_k(t)} \delta(t - \tau_k(t)) \tag{2.2}$$

which is the more general case of the impulse response as developed by Turin in [27] using measured power delay profiles. This model describes the paths (or rays) by their real positive gains $\{\beta_k\}$, propagation delays $\{\tau_k\}$, and phase shifts $\{\theta_k\}$ for the k^{th} ray, $k \in [0, \infty)$, where $\delta(\cdot)$ represents the Dirac delta function and τ_0 denotes the arrival time of the first observed event.

Because of the scatterer motion already mentioned, the parameters β_k, τ_k and θ_k are randomly time-varying functions, as indicated by (2.2). However, the movement in the building is slow, so it is expected that the parameters' rates of variation are very small relative to signaling rates of more that a few tens of kbits per second (kbits/s). The channel is even considered wide-sense stationary for periods of time up to at least 2 seconds [28]. The parameters are thus considered to be virtually time-invariant random variables for the case of data rates in the order of Mbits per second (Mbits/s). This is also motivated by the fact that the maximum Doppler frequency is only in the order of 10^{-5} times the bit rate for a signaling rate of several hundred kbits/s. The Doppler frequency f_D is defined as:

$$f_D = \frac{V}{\lambda_c}, \tag{2.3}$$

where V is the mobile unit's velocity (on the order of a few metres per second or less) and λ_c is the wavelength (0.2 m for $f_c = 1.5$ GHz) [29].

Statistical Definition of Model Parameters

A simple yet complete discrete statistical model is described by Saleh and Valenzuela [24] as a special case of the general model of equation (2.2). It is observed that rays arrive in clusters. This is better modeled by the modified complex low pass impulse response:

$$h(t) = \sum_{l=0}^{\infty} \sum_{k=0}^{\infty} \beta_{kl} e^{j\theta_{kl}} \delta(t - T_l - \tau_{kl}) \tag{2.4}$$

where l is the cluster index and k is the ray index in the l^{th} cluster. Figure 2.1 gives a general representation of this model.

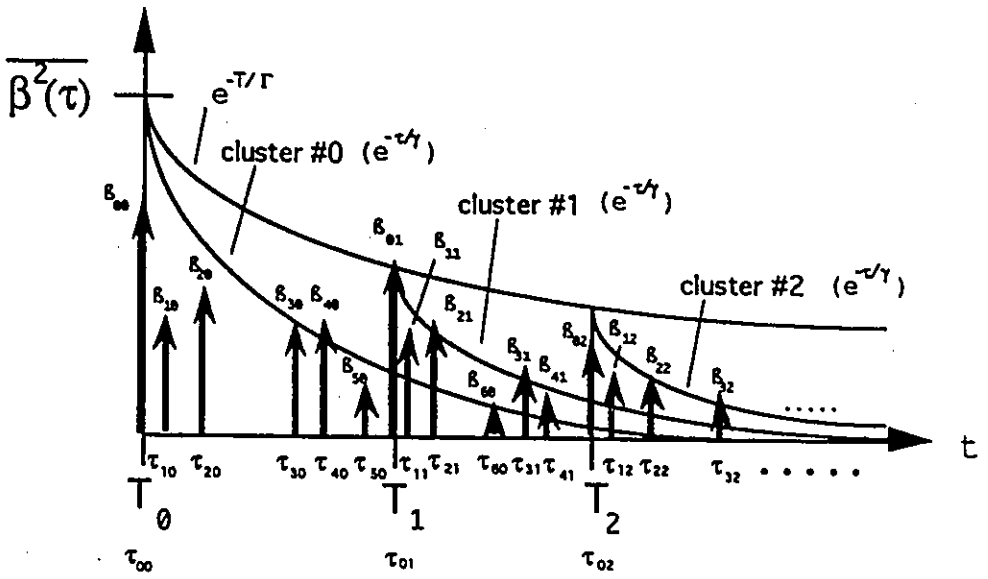

Figure 2.1: Representation of the discrete indoor wireless channel model.

The phase angles $\{\theta_{kl}\}$ are assumed *a priori* to be statistically independent random variables with uniform distributions over $[0, 2\pi)$. The arrival times $\{T_l\}$ of the l^{th} cluster and $\{\tau_{kl}\}$ of the k^{th} ray (measured from the beginning of the l^{th} cluster) form Poisson arrival-time sequences with mean arrival rates Λ and λ respectively, and are

described by the independent interarrival exponential probability density functions:

$$p(T_l|T_{l-1}) = \Lambda \exp[-\Lambda(T_l - T_{l-1})]u(T_l - T_{l-1}) \qquad l > 0 \tag{2.5}$$

$$p(\tau_{kl}|\tau_{(k-1)l}) = \lambda \exp[-\lambda(\tau_{kl} - \tau_{(k-1)l})]u(\tau_{kl} - \tau_{(k-1)l}) \qquad k, l > 0 \tag{2.6}$$

The clusters are found to generally overlap. The path gains $\{\beta_{kl}\}$ are chosen to be statistically independent Rayleigh distributed random variables with the mean square values $\{\overline{\beta_{kl}^2}\}$ monotonically decreasing functions of $\{T_l\}$ and $\{\tau_{kl}\}$. The density function for the path voltage gain is:

$$p(\beta_{kl}) = \frac{2\beta_{kl}}{\overline{\beta_{kl}^2}} \exp\left(\frac{-\beta_{kl}^2}{\overline{\beta_{kl}^2}}\right) u(\beta_{kl}) \tag{2.7}$$

with the mean square value obtained as:

$$\overline{\beta_{kl}^2} = \overline{\beta^2(0,0)} \exp(-T_l/\Gamma) \exp(-\tau_{kl}/\gamma) \tag{2.8}$$

where $\overline{\beta^2(0,0)} = \overline{\beta_{00}^2}$ is the average power gain of the first ray of the first cluster, and Γ and γ are power-delay time constants for the clusters and rays, respectively.

Furthermore $\overline{\beta_{00}^2}$ is obtained from the average multipath power gain $\overline{G}(r)$:

$$\overline{G}(r) = \gamma\lambda \, \overline{\beta^2(0,0)} \sum_{l=0}^{L} \exp(-T_l/\Gamma) \tag{2.9}$$

as:

$$\overline{\beta^2(0,0)} \approx (\gamma\lambda)^{-1} G(1\text{m}) \, r^{-\alpha} \tag{2.10}$$

where r is the antenna separation (in metres), α is the distance-power law exponent, and $G(1$ m$)$, the multipath power gain at an antenna separation of $r = 1$, is given approximately by:

$$G(1\text{m}) \approx P_{rec}/P_{trans} = G_t G_r (\lambda_c/4\pi r)^2|_{r=1} \tag{2.11}$$

where P_{rec}/P_{trans} is the free-space power transmission ratio, G_t and G_r are the gains of the transmitting and receiving antennas respectively, and λ_c is the RF wavelength. Both antennas are located at a height of about 2 metres from the floor for all published results mentioned.

The following values are used in [24]:

$$\begin{aligned} G_t &= G_r \approx 1.6 \\ \lambda_c &= 0.2 \text{ m for } f_c = 1.5 \text{ GHz} \\ r &= \text{variable} \end{aligned}$$

By fitting the measurements to this model, it is determined [24] that:

α	γ (ns)	Γ (ns)	$1/\lambda$ (ns)	$1/\Lambda$ (ns)
3	20	60	5	300

The distance-power law exponent α, which has a value of 2 in free space, depends on the building structure and its construction materials [30, 31, 32]; reported values vary between 1.2 and 6.5. A value of between 2 and 4 seems to describe well an average office with plasterboard walls, with lower values possible when the line-of-sight (LOS) cases are considered [28].

Given these statistics, it is simple to generate the parameters $\{\theta_{kl}\}$, $\{T_l\}$, $\{\tau_{kl}\}$ and $\{\beta_{kl}\}$ and obtain a typical discrete low-pass impulse response for the IW channel.

Other Model Issues

This model's parameter development excluded hallway measurements because these have an LOS component as well as strong components with long delays, which are not necessarily typical of most office environments.

Other distributions could fit the data as well or better than the Rayleigh distribution, however it is believed that it is much simpler to work with Rayleigh distribution in the analysis because it is "quite adequate for the model" [24]. Not surprisingly, some studies report a Rician distribution for the path gains because the LOS cases are not ignored [28]; others present what is considered to be a more accurate modified Poisson process to describe ray arrivals and show that a log-normal distribution is better than the Rayleigh distribution to describe the path gains [33].

A more recent model is the autoregressive frequency domain statistical model as described by [34], which is developed to have very few parameters, that is, considerably less than the time domain model presented. This model represents the channel impulse response in the z-domain as a linear filter with transfer function:

$$H(z) = \prod_{i=1}^{P} \frac{1}{(1 - p_i z^{-1})} \tag{2.12}$$

where two poles ($P = 2$) are found to be sufficient to accurately model the response. This leaves the two complex values (p_1, p_2) as the only channel parameters. The two poles can be interpreted as two clusters of multipath arrivals, and their distance from the unit circle as the power of the cluster. This interesting model is not mentioned any further in this work, except briefly at the end.

A commercial indoor micro-cellular radio channel simulator [35] that runs on a PC computer has appeared recently on the market. It can be used for simulations such as are described further in this work, to study coding and equalization techniques. This is also briefly mentioned again at the end.

2.3 RMS Delay Spread

The channel impulse response is completely characterized by the delay spread function $\rho(\tau)$ [36], but since measurements of this function are not available, and the maximum data rate (and therefore the system performance) for a given building depends primarily on the square root of the second moment of the power delay profile, the latter measure is used to characterize the impulse response [36]. Also known as the rms delay spread, the square root of the second moment for the discrete case, modified from [37] for the present case of rays in clusters, is given as:

$$\sigma_T = \sqrt{\frac{\sum_{k=1}^{K}\sum_{l=1}^{L}(T_l + \tau_{kl} - \overline{\tau})^2 P(T_l + \tau_{kl})}{\sum_{k=1}^{K}\sum_{l=1}^{L} P(T_l + \tau_{kl})}} \tag{2.13}$$

for L clusters with a maximum of K rays in each, where $P(T_l + \tau_{kl})$ is the power delay profile, with the average delay $\overline{\tau}$:

$$\overline{\tau} = \frac{\sum_{k=1}^{K}\sum_{l=1}^{L}(T_l + \tau_{kl}) P(T_l + \tau_{kl})}{\sum_{k=1}^{K}\sum_{l=1}^{L} P(T_l + \tau_{kl})} \tag{2.14}$$

where $\tau_{0l} = 0$ by definition, so that each cluster starts with a ray.

The normalized rms delay spread σ_N is a useful measure when comparing the performance of systems operating at different data rates, and can be used to indicate the severity of the frequency selective fading [8]. It is defined as

$$\sigma_N = \frac{\sigma_T}{T_s} \tag{2.15}$$

with T_s being the symbol period.

Published rms delay spread values obtained from measurements are given in Table 2.1 for various building types, including offices, residences and factories. It is found that a good direct path can have a considerable effect on the rms delay spread in an office environment by reducing the worst case value below 100 ns [39, 40, 41, 42].

Source	*Building Type*	*Mean* (ns)	*Maximum* (ns)
Saleh & Valenzuela [24][1]	office	25	50
Ganesh & Pahlavan [33]	office	55	146
Devasirvatham [38]	office	125	250
Devasirvatham [39, 40][2]	office	—	321
	residence	220	422[3]
Devasirvatham [41, 42]	small office	60	218[4]
	large office	120	250[5]
Rappaport [43, 44]	factory[6]	105	300

Table 2.1: Comparison of Published RMS Delay Spread σ_T Measurements.

Making the receiver more visible from all sections of the office floor is thus desirable to minimize the spread and attenuation of the signal, however this is not always practical, and so the system must sometimes deal with large values of rms delay spread.

The rms delay spread range is thus taken to be from about 10 ns up to about 250 ns for an office environment, with a mean of about 55 ns and 120 ns for small and large office environments respectively, where strong LOS paths between the transmitting and receiving antennas are not considered common.

As mentioned, the rms delay spread limits the maximum data rate because of ISI. In a multipath channel, the data rate is upper bounded to a value that is inversely proportional to the maximum rms delay spread, unless countermeasures are used to reduce its effect. The proportionality is a function of the modulation scheme and the transmit and receive filters used, among other factors.

[1] Occasional measurements of up to 150 ns were excluded because they represented hallway measurements, which were not considered common in office environments.

[2] Measurements carried out from inside to outside of building.

[3] Reduces to below 100 ns with LOS path. These large values are for a condominium complex with no line of sight.

[4] Reduces to below 70 ns with LOS path.

[5] Reduces to below 88 ns with LOS path.

[6] RMS delay spread does not appear to depend on LOS path in factories.

For example, with BPSK and a rectangular signal spectrum of width $1/T_b$, where T_b is the bit period, the maximum data rate for a 10^{-4} outage probability at a 10^{-4} BER is only 0.0022 times the inverse of the rms delay spread, whereas with QPSK and raised cosine signal spectrum of the same bandwidth as the BPSK signal, the maximum data rate is increased six-fold [5], or about 0.013 times the inverse of the rms delay spread.

The effect of the carrier frequency on the IW channel propagation characteristics is studied in [45]. The standard deviation of the rms delay spread increases for a carrier frequency of $f_c = 1.75$ GHz compared with $f_c = 910$ MHz. This indicates a less uniform coverage for higher carrier frequencies.

2.4 Channel Impairment Countermeasures

Methods to reduce the effect of slow-fading and dispersion include interleaving, diversity, coding and equalization. Interleaving is shown to be unsuitable for the slow-fading of the IW channel. Diversity is useful to reduce the impact of fading, and is normally required to ensure acceptable performance. Coding and equalization are studied in the next chapter.

2.4.1 Interleaving

Interleaving typically helps to reduce the effects of burst transmission errors by redistributing them more uniformly, and is normally applied to fast-fading channels since during fades, errors tend to occur in bursts. Its effectiveness for the slow-fading IW channel is reduced considerably since the fades can last for long periods of time, creating excessively long error bursts that require an interleaver of considerable size. This is prohibitive in system complexity and interleaving/de-interleaving delays. For these reasons, interleaving is not considered.

2.4.2 Diversity

N-branch diversity is based on obtaining the transmitted information from N waveforms received over N independently fading channels. The objective is to combine these received signals in such a way that the effect of fading and random antenna orientation will be noticeably reduced. Several ways to achieve diversity exist and they are all designed for very low correlation between the N received signals. Two uncorrelated signals going through deep fades at the same instant is not a very probable occurrence, so the resulting combination reduces the probability of fading.

The slow-fading that occurs in the IW channel can cause signal loss for periods on the order of up to seconds or minutes, which can cause errors over millions of bits. This is not acceptable for data communications, therefore diversity must be used in such a system to achieve acceptable performance. Diversity can also be used to increase the possible signaling rate for a given maximum rms delay spread [9]. An overview of the major diversity techniques follows. A few more techniques are mentioned in [26, 29, 46].

Frequency diversity has the same information transmitted on N different carrier frequencies spaced to achieve acceptable decorrelation between them. This method is avoided because it is spectrally inefficient.

Time diversity has the information transmitted in N different time slots over the same carrier frequency. For the slowly varying IW channel, the time separation required to decorrelate the signal variations in the different time slots is excessive and so this technique is also dismissed.

Space (or antenna) diversity uses N receiving antennas spaced sufficiently far apart (normally $\lambda_c/4$ to $\lambda_c/2$) so that the received signals are uncorrelated and thus fade independently. This is spectrally efficient.

Polarization diversity relies on the independence of signals received over orthogonally polarized antennas. This is both spectrally and spatially efficient.

The advantages of antenna diversity with cordless telephones [47] and wide-band indoor wireless networks [4, 5, 36] are reported, such as reducing the effects of spreading, fading and random orientation. Antenna diversity applied only to the central port unit [4] is considered to reduce size and complexity of portable units, and is implemented in a design that uses four dipoles spaced one-quarter wavelength ($\lambda_c/4$) apart [48], where upon reception at the base station, one of the four uncorrelated signals is chosen, and during transmission, one of the four antennas is used to guarantee service at rates of 10 Mbits/s. As an example, to achieve 10^{-4} outage probability at a 10^{-4} BER, a system using 4-branch antenna diversity with maximal-ratio combining and QPSK has nearly 150 time the maximum data rate of a BPSK system without diversity [36].

Polarization diversity is also useful to reduce the effect of fading in the indoor wireless channel [49].

2.5 Summary

The indoor wireless channel and its impairments are presented. A previously available statistical model is explained and the rms delay spread is shown to be an important characteristic measure of the IW impulse response.

Techniques to reduce the channel impairments' effects on the transmitted signal are mentioned, such as interleaving, which is not recommended in a slow fading channel, and diversity, which should be considered in the design of any indoor wireless communication system, using either space or polarization techniques. Coding and equalization, briefly mentioned, are dealt with in depth in the next chapter.

Chapter 3

Coding and Equalization

As mentioned in the previous chapter, coding and equalization methods may be used to reduce the channel impairments, such as fading and dispersion, that occur with indoor wireless propagation.

Conventional error control coding techniques, using either block codes or convolutional codes to improve performance, are very well documented in the literature, as in [50]. Such codes operate on the discrete channel using a rate R_c encoder, and the two functions of coding and modulation required at the transmitter are usually considered as separate operations.

The encoder outputs n coded bits given k input bits, where $k/n < 1$. The n-bit coded output, represented as a coded symbol, is mapped by the modulator onto a set of M possible signals. The demodulator then attempts to recover these n bits by making an independent M-ary nearest neighbour (hard) decision on each received signal. The decoder in turn decodes these n bits using the Hamming distance as the metric for its decisions, and recovers an estimate of the k original bits.

The use of such an encoder dictates either a decrease in the information rate or an increase in bandwidth. Supposing that bandwidth efficiency is a consideration in the design, these drawbacks can be avoided by expanding the signal set of the modu-

lator, but the trade-off here is decoder complexity and reduced decision regions. This leads to unsatisfactory results, as a coded system with an expanded signal set performs worse than its uncoded counterpart [51] because reduced decision regions means that the signals are closer in the constellation mapping, thus increasing the possibility of a wrong decision. Conventional coding techniques cannot then be directly applied in conjunction with band-limited modulation techniques to achieve significant performance gains [52], because independent hard-decisions are made by the demodulator before decoding occurs. Soft-decision decoding must be used to achieve performance gains of consequence.

Combined coding and modulation schemes, or coded modulation, which use specially designed codes, can be used in this instance to achieve even greater performance gains. Such schemes can use trellis codes, and if so are termed trellis-coded modulation (TCM). TCM with PSK is used in this particular study in order to establish a measure of its performance when applied to the IW channel, relative to an uncoded system.

A brief review of some of the studies done with other modulation schemes applied to the IW channel is first presented in Section 3.1. TCM performance is compared to uncoded modulation performance, so PSK is discussed briefly in Section 3.2. This is followed by a detailed description of TCM in Section 3.3 as designed for the Gaussian and fading channels, and a presentation of its performance as reported in the literature for the additive white Gaussian noise channel. A brief description of the Viterbi algorithm, used as the decoder, is also presented.

Performance degradation due to ISI occurs in the IW channel, and equalization uses filters to compensate for the interference distortions. A fringe benefit of using equalization to reduce ISI is that it also provides an implicit multipath diversity by adding the spread components of each symbol together with weighting. Equalization

is studied in Section 3.4 for the case of multipath channel and coded modulation. Differential detection considerations for TCM and equalization are mentioned.

3.1 Review of Published Modulation Results

A brief review is presented of studies found in the literature, discussing different modulation schemes applied to the IW channel.

Coherent 4-QAM is studied for various bit rates R_b ranging from 1 Mbits/s to 64 Mbits/s using space diversity [14, 15], and it is found to perform at rates of 1 Mbits/s with an outage probability of $< 10^{-3}$ at a BER of $< 10^{-4}$, when considering an rms delay spread of 100 ns and using an adaptive minimum mean square error (MSE) equalizer. The situation without equalizer shows that two-antenna diversity can achieve the same performance for a reduced rms delay spread of 25 ns.

A comparison of BPSK, QPSK, 8-PSK, OQPSK and MSK for normalized rms delay spreads σ_N below 0.2 (i.e. $\sigma_T < 40$ ns for QPSK with bit rate R_b =10 Mbits/s) shows that QPSK and 8-PSK are more resistant to delay spread, and that there is no improvement from QPSK to 8-PSK for large SNR [8, 9]. As can be expected, an increase in the rms delay spread or the bit rate R_b will cause increasing ISI impairments. It is also found that coherent detection performs better than differential detection [8, 9, 10] since differential detection suffers from large effective rms delay spread due to two consecutive dispersive waveforms being mixed together at the detector. Thus coherent QPSK leads to better performance results, relative to other PSK schemes.

Direct sequence spread spectrum (DS-SS) with non-coherent demodulation is considered for an IW LAN [16, 17, 18] because of the spread spectrum's inherent diversity. For a 32 kbits/s packet speech application using 1kbit packets and a BER of around 10^{-4}, it is found that for an increase in rms delay spread from 100 to 250 ns, a system

using selection diversity with error coding suffers from a decrease in the number of simultaneous users by up to 20%, and a system with maximal ratio combining sees an increase in the number of simultaneous users of up to nine times; this is due to the increased inherent diversity [17]. This diversity permits the system to operate error-free for signal fade notches of 10 dB and 20 dB [18], fades which would make synchronous carrier recovery a rather difficult task. Thus, contrary to non-spreading schemes, impairment caused by ISI does not increase for increases in rms delay spread within a certain range. It is also found that SS performance is robust to various channel models [16], so it is expected to also be robust to the varying IW channel. Also, [18] seems to indicate that SS doesn't suffer from an irreducible BER floor as the SNR is increased, unlike other modulation schemes.

Slow frequency hopping and error coding are successfully combined with TDMA and FSK modulation in a flexible system [12, 13] that effectively combats fading and interference when operating at a data rate of 1 Mbit/s. For an rms delay spread of 25 ns and a block failure rate of 10^{-4}, the outage probability obtained is between 2×10^{-4} and 10^{-5}, when using a code that corrects two symbol errors.

Infrared communication systems using various modulation techniques, including spread spectrum, are considered in [53]. Infrared radiation is restricted to LOS reception in the room in which it is generated, so it would be unsuited to an IW LAN, which should cover many rooms.

A distributed antenna (or "leaky feeder") set-up for broadband TDMA-type systems is proposed in [54] to reduce both signal attenuation and rms delay spread by keeping all mobile units close to the fixed station antenna. This causes the rays to appear in one dominant cluster. A distributed antenna system with 6 m separation between antennas has its maximum rms delay spread cut by a factor of two, compared

to a one antenna set-up. Such a system is virtually building-independent if properly distributed.

3.2 Phase Shift Keying

Discrete phase modulation, known as M-ary phase shift keying (M-PSK), is the most frequently used digital modulation technique, and is used as reference in this study. It consists of mapping m bits represented as a symbol onto one of $M = 2^m$ possible signals. These signals can be described as low pass waveforms:

$$u_m(t) = \sqrt{\frac{2E}{T}} e^{j2\pi(m-1)/M} \quad \begin{matrix} m = 1, 2, \ldots, M \\ 0 \leq t \leq T_s \end{matrix} \tag{3.1}$$

The information is carried on the phase of the waveform.

The scheme presented as a reference is QPSK, where two-bit symbols are mapped onto one of four waveforms. Gray code mapping is used to make sure that adjacent symbols in the mapping differ by only one bit, so the most likely single symbol error corresponds to a single bit error.

Demodulation can occur in one of three ways [55]: (1) M-PSK: coherent demodulation that requires carrier phase and frequency recovery circuits. This may introduce a phase ambiguity. (2) M-DEPSK: a differential encoder is used at the modulator and differential decoding at the demodulator is performed on the regenerated data stream by means of logic circuitry [55, p.169]. This also requires carrier recovery circuits but solves the phase ambiguity. Note that the coding can be applied on all or only a selected number of bits to solve the ambiguity [56, 57]. (3) M-DPSK: differential encoding is applied at the modulator and comparison demodulation is performed on the modulated signal using a differential detector that replaces the carrier recovery circuit. This improves the synchronization speed of the demodulator, and reduces its

complexity, but it also reduces performance and the recovery becomes non-coherent.

The probability of bit error performance for the various QPSK systems with Gray coding is as follows [55]:

$$P_{b_{QPSK}} = \frac{1}{2}\text{erfc}\sqrt{\frac{E_b}{N_0}} \tag{3.2}$$

$$P_{b_{DEQPSK}} = \text{erfc}\sqrt{\frac{E_b}{N_0}} \tag{3.3}$$

The probability of bit error performance for DQPSK with Gray coding is given [26] as:

$$P_{b_{DQPSK}} = Q(a,b) - \frac{1}{2}I_0(ab)e^{-(a^2+b^2)/2} \tag{3.4a}$$

where:

$$a = \sqrt{2\frac{E_b}{N_0}(1-\frac{1}{\sqrt{2}})} \tag{3.4b}$$

$$b = \sqrt{2\frac{E_b}{N_0}(1+\frac{1}{\sqrt{2}})} \tag{3.4c}$$

$$Q(a,b) = e^{-(a^2+b^2)/2}\sum_{k=0}^{\infty}\left(\frac{a}{b}\right)^k I_k(ab) \tag{3.4d}$$

and $I_k(x)$ is the k^{th} order modified Bessel function of the first kind. Figure 3.1 presents the probability of bit error performances for these three cases in the Gaussian channel. It is seen that differential detection has a performance penalty of almost 3dB over coherent detection.

3.3 Trellis-Coded Modulation

As mentioned previously, a coding gain cannot be expected if conventional coding techniques with an expanded signal set are applied to a band-limited channel with hard-decisions taken at the demodulator. Soft-decision decoding and specially designed codes must be used.

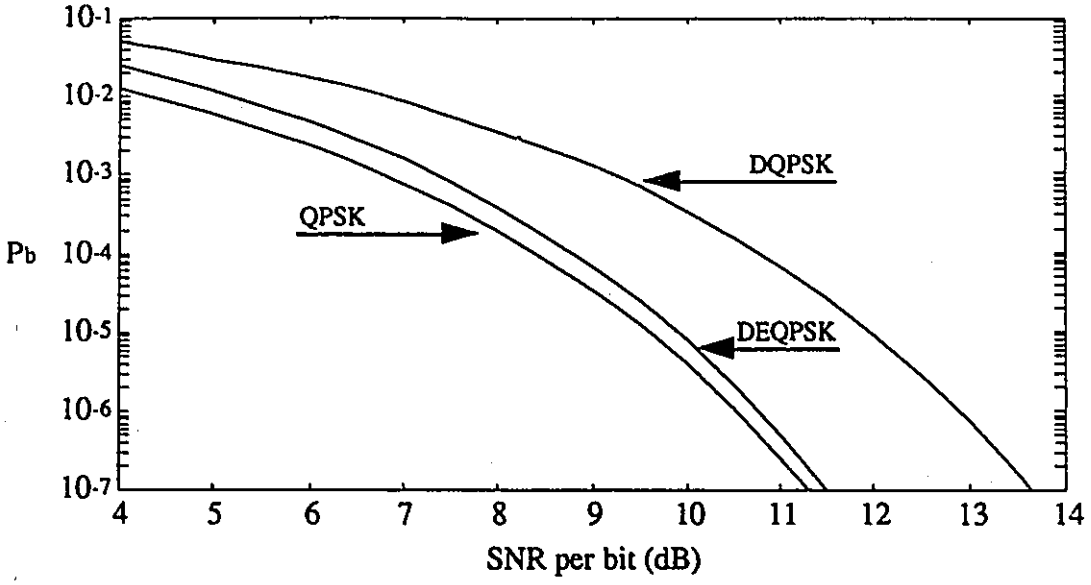

Figure 3.1: Probability of bit error performance for various QPSK schemes.

3.3.1 Trellis-Coded Modulation for Gaussian Channels

It is known that soft-decision decoding requires the Euclidean distance as the metric of decision instead of the Hamming distance, but the mapping of symbols from a code optimized for Hamming distance doesn't necessarily lead to a good Euclidean distance structure. In fact, Hamming and Euclidean distances are equivalent only in the case of binary or four phase modulation. The codes must therefore be specially designed to achieve maximum free Euclidean distance between encoded sequences.

For the signal set expansion, it is found that by doubling the number of channel signals, almost all is gained in terms of the channel capacity [56]. This leads to an encoder rate $R_c = m/(m+1)$ with m input bits, and the mapping of $(m+1)$-bit symbols onto a set of $M = 2^{(m+1)}$ signals, as shown in Figure 3.2, using familiar multilevel/phase techniques to increase the information rate.

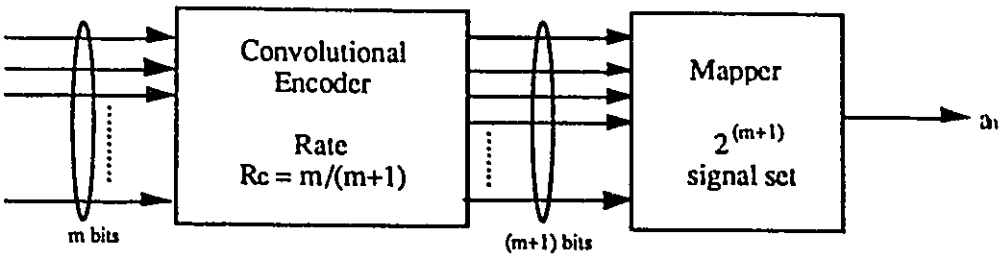

Figure 3.2: TCM modulator: convolutional encoder and mapper.

The design criteria is the maximization of the free Euclidean distance (ED):

$$d_{free} = \min_{\{a_n\} \neq \{a'_n\}} \left[\sum_n d^2(a_n, a'_n) \right]^{\frac{1}{2}}, \tag{3.5}$$

where $d(a_n, a'_n)$ denotes the ED between channel signals $\{a_n\}$ and $\{a'_n\}$; a_n and a'_n represent any of the $2^{(m+1)}$ discrete channel input signals.

The design method aimed at increasing free ED is based on "mapping by set partitioning" [56]. This mapping follows from successive partitioning of the signal set into subsets with increasing minimum distance $\Delta_0 < \Delta_1 < \Delta_2 \ldots$ between the signals of these subsets. This is illustrated in Figure 3.3 for the case of 8-PSK.

Both block and convolutional coding can be used, but any coding scheme that can be achieved with a block code can also be achieved with greater simplicity and better performance using a convolutional code [52, 58], hence the choice of convolutional codes. The convolutional encoder of interest can be thought of as a finite-state machine with m-bit inputs and ν binary storage elements representing 2^ν possible states and 2^m possible transitions from each state to a successor state; ν is called the code constraint length. The encoder can also be represented by a trellis diagram, whose most important property is that for every possible path through it, there is a corresponding unique state sequence, and vice versa. Trellis coding introduces redundant signal points and codes

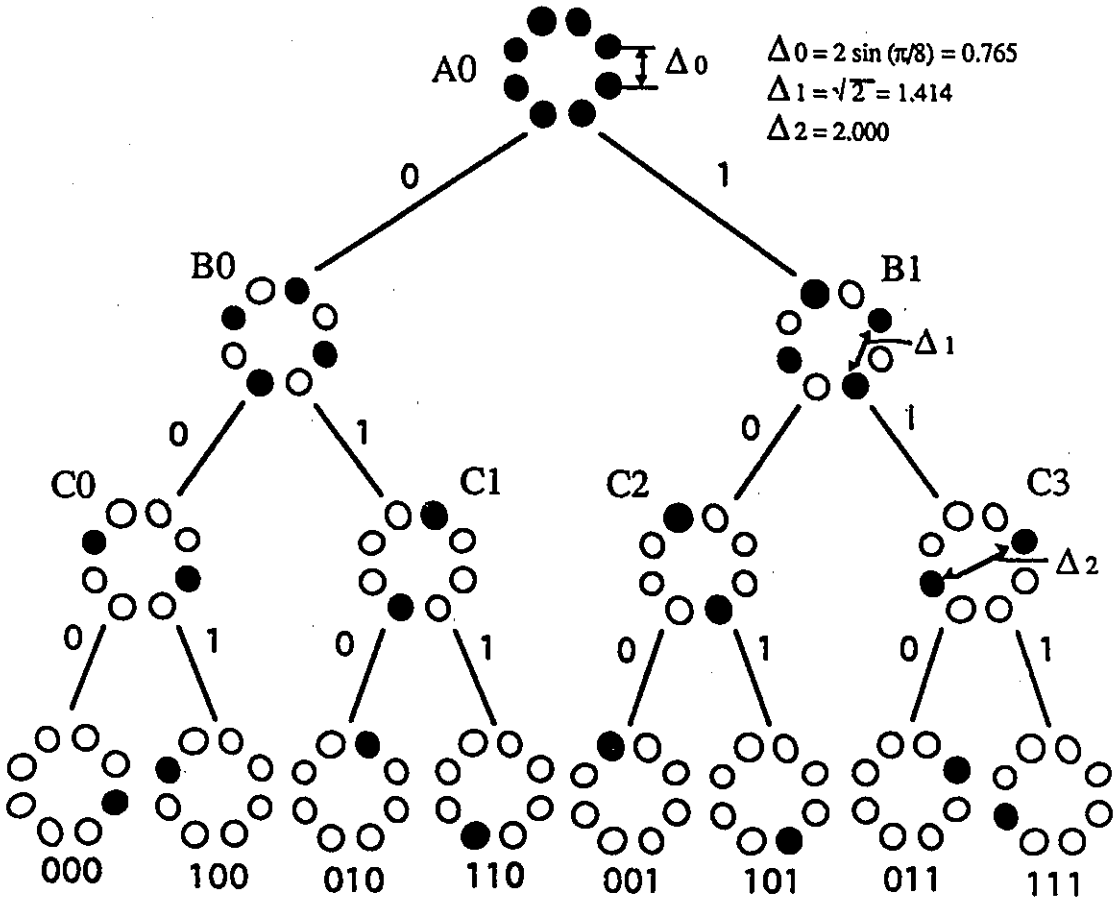

Figure 3.3: Mapping by set partitioning for 8-PSK.

the signal set in such a way as to make the error events depend on the Euclidean distance of signal paths (i.e., between encoded sequences) rather than signal points [58]. Once a suitable trellis state-transition diagram is chosen, the expanded signal set must be assigned to the transitions in such a way that maximizes free ED. The rules for assigning transitions in the trellis are summarized as follows:

- All parallel transitions in the trellis structure receive the maximum possible Euclidean distance in the signal constellation (distance $\Delta_n = \Delta_2$ for 8-PSK in Figure 3.3).

- All transitions diverging from or merging into a trellis state receive the next maximum possible Euclidean distance (distance $\Delta_{n-1} = \Delta_1$ for 8-PSK).

This second step is repeated until all transitions have been defined (distances $\Delta_{n-2}, \Delta_{n-3}, \ldots, \Delta_0$). This can be done by hand for simple codes, or by computer for larger codes [56].

The presence of parallel transitions implies that single signal error events can occur. This limits the maximum free ED to the minimum distance in the subsets of signal assigned to parallel transitions, but on the other hand it reduces the trellis connectivity [51, 59].

It is important to note that the specific mapping of coded symbols into channel signals is not important. By permuting subsets, other mappings can be obtained with the same pattern of increasing minimum subset distances [56]. Also, the traditionally used Gray code generally does not provide the best mapping for coded systems.

3.3.2 Decoding with the Viterbi Algorithm

Optimum decoding in this case involves finding a signal sequence that most closely corresponds to the sequence of transmitted signals. A decoding metric $d(\mathbf{x}, \mathbf{r})$ is calcu-

lated between $\mathbf{x}$ and $\mathbf{r}$ where $\mathbf{x} = (x_1, x_2, \ldots, x_J)$ is a possible sequence of transmitted signals and $\mathbf{r} = (r_1, r_2, \ldots, r_J)$ is the received sequence. The metric is a non-negative function of $\mathbf{x}$ given $\mathbf{r}$, and is related to the conditional probability that $\mathbf{x}$ was transmitted if $\mathbf{r}$ was received. The decoder then chooses the message sequence $\mathbf{x}$ for which this metric is minimized. It makes an error if it decodes a sequence $\mathbf{x}'$, given that the correct transmitted sequence is $\mathbf{x}$. This happens if $d(\mathbf{x}', \mathbf{r}) \leq d(\mathbf{x}, \mathbf{r})$.

The Viterbi algorithm (VA) is a maximum-likelihood sequence estimation (MLSE) procedure that finds the symbol sequence which is closest to the transmitted symbol sequence [50, 60, 61] efficiently. Over one path, the 2^m branch metrics are calculated for each 2^ν states and one survivor is chosen for each state. This ensures that only 2^ν paths and their corresponding metrics need to be stored in memory. It is a recursive procedure that does the following:

(a) for the 2^ν states, compute the 2^m branch metrics $d(x_{ij}, r_j) = |x_{ij} - r_j|^2$ which represent the Euclidean distances between the complex received signal r_j at discrete time j and the i^{th} complex symbol x_{ij} associated with a transition in the trellis $(1 \leq i \leq 2^m)$.

(b) add the respective branch metrics to the survivor metrics to determine the cumulative path metrics.

(c) determine the survivor for each state by selecting the path corresponding to the smallest metric among the extended path metrics.

(d) repeat (a), (b) and (c) for $1 \leq j \leq J$.

(e) the survivors should have merged into one path for most of the sequence, except maybe for a few symbols at the end. If they do merge, the resulting path is the decoded sequence; otherwise a decision must be taken to choose

one of the 2^{ν} survivors as the decoded sequence. This decision may be done arbitrarily.

Thus at any discrete time j, the 2^{ν} survivors' paths and their metrics are stored in memory.

Merging is a random phenomenon, and without truncation, it is possible that no decisions can be made until the end of the entire sequence, which for certain situations can be never. Since the decoder cannot usually wait until the end of the transmission to make a decision, it is necessary to truncate survivors to some manageable length D, called decoding depth, and then force a decision. At time j, a decision is forced on the symbol received at time $(j - D)$, using information from symbols received up to the present time j. The stored surviving paths are only for the last D symbols since all symbols up to the $(j - D - 1)^{th}$ have been chosen, and hence decoded into information symbols.

The additional error probability due to truncation is negligible if there is a high probability that at time j all survivors go through the same node up to time $(j - D)$. This means that the initial segment of the maximum-likelihood path is known up to time $(j - D)$ and is taken as the decision at the truncation. If the survivors disagree, any reasonable strategy to make the decision will work if D is large.

Generally, the decoding depth D is chosen large enough so that this additional error probability due to truncation is negligible. For small SNR, a minimum truncation length of $D \approx 5.8\nu$ is found to achieve this negligibility objective [50, 62]. If D is chosen too large, the incurred delay may be excessive for the user.

When the transmitted sequence becomes very long, the metrics can become quite large. It is necessary to normalize them regularly by subtracting a constant from all

of them in order to avoid overflow.

Because of its highly parallel structure and need for only add, compare and select operations, the Viterbi algorithm is well suited to high-speed applications [60]. A 115 Mbits/s Viterbi decoder custom chip has been developed [63] for the rate $R_c = 2/3$, 4-state 8-PSK trellis code. It uses parallel processing on the bit level to reduce throughput rate bottlenecks due to the add-compare-select recursion. Both Qualcomm Inc. and Stanford Telecom presently offer Viterbi decoding chips that operate beyond 10 Mbits/s; though these are unsuited for TCM, one can realistically expect a commercial high speed Viterbi decoder chip for TCM in the near future.

3.3.3 Performance of Trellis Coded Modulation

Different performance measures can be used to characterize a given code. Some of these have been mentioned previously.

1. d_{free}: the minimum Euclidean distance between all possible pairs of code sequences.

2. $N(d_{free})$: the number of error sequences with distance d_{free}; for a given sequence (usually chosen to be the all-zero sequence), it represents the number of neighbours with distance d_{free}, and hence those with which it is more likely to be confused and cause errors.

3. P_b: bit error probability.

4. P_E: event error probability. An event error occurs whenever the received symbols are closer in Euclidean distance to some alternative sequence than to the actually transmitted sequence.

5. G: coding gain; the difference between the values of SNR (in dB) necessary to achieve the same P_b in the uncoded and coded systems. The asymptotic coding gain in decibels is given as:

$$G|_{SNR\to\infty} = 10\log_{10}\left(\frac{d_{free}}{d_{UC}}\right)^2 \tag{3.6}$$

where d_{UC} is the minimum distance of the uncoded scheme.

These performance measures can be obtained from [59], where upper and lower bounds and asymptotic estimates are given for the error probabilities. The lower bound asymptotic estimate is given in [51, 58, 59] as:

$$P_b \geq \frac{1}{2}N(d_{free})\ \mathrm{erfc}\left(d_{free}\sqrt{\frac{E_b}{N_0}}\right) \tag{3.7}$$

where E_b is the received signal energy per bit, N_0 is noise power density. The upper bound applies the code's generating function [50, 64] to the union bound. It can also be obtained using:

$$P_E \leq \sum_{d=d_{free}}^{\infty} N(d)P_E(d) \tag{3.8}$$

where $N(d)$ is the number of sequences with distance d, and $P_E(d)$ is the first-event error probability corresponding to the Euclidean distance d [50, p.324].

For the simple 4-state and 8-state 8-PSK codes considered in this study, d_{free} and $N(d_{free})$ are easily found by inspection of the trellis, but for larger trellis codes, this becomes complicated, so computer search methods are available. The three codes considered are shown in Figures 3.4 to 3.6, and are easily generated using binary convolutional encoders of rate $R_c = 2/3$. Uncoded QPSK, used as the reference because it requires the same bandwidth as coded 8-PSK, can be viewed as coding with only one state and four parallel transitions, where $d_{free} \equiv \Delta_1 = 1.414$. The 4-state 8-PSK with parallel transitions in Figure 3.4 has $N(d_{free}) = 1$ (one path: 4) with $d_{free} \equiv \Delta_2 = 2.0$.

The 4-state 8-PSK with distinct transitions in Figure 3.5 has $N(d_{free}) = 2$ (two paths: **2-0-1** and **6-5**) with $d_{free} \equiv \sqrt{\Delta_1^2 + \Delta_0^2} = 1.608$. The 8-state 8-PSK in Figure 3.6 has $N(d_{free}) = 2$ (two paths: **2-0-1-2** and **6-7-6**) with $d_{free} \equiv \sqrt{\Delta_1^2 + \Delta_0^2 + \Delta_1^2} = 2.141$. These represent asymptotic coding gains in free ED of 3.0, 1.1 and 3.6 dB respectively over the uncoded 4-PSK.

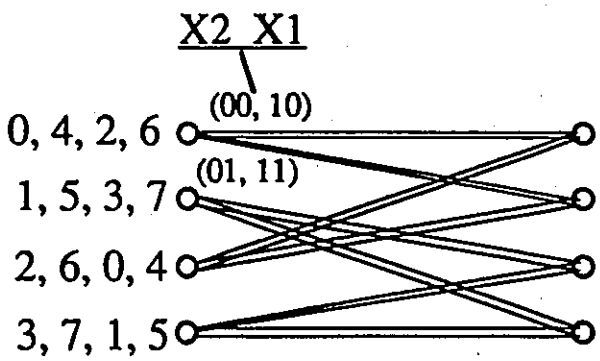

Figure 3.4: Four-state 8-PSK trellis with parallel transitions.

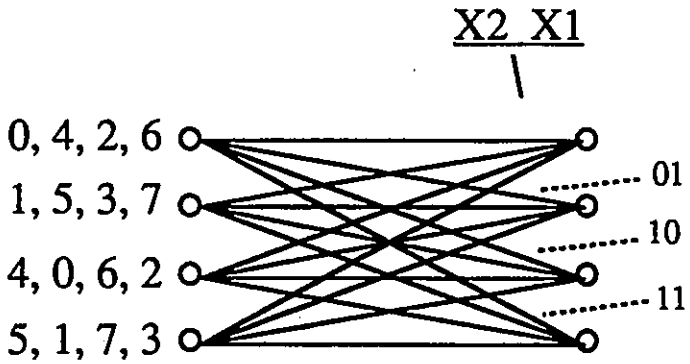

Figure 3.5: Four-state 8-PSK trellis with distinct transitions.

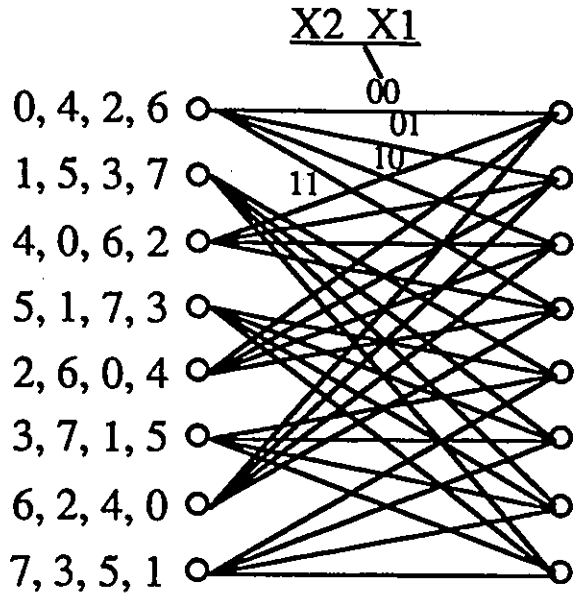

Figure 3.6: Eight-state 8-PSK trellis with distinct transitions.

The best 4-state 8-PSK code has parallel transitions (i.e., 3 dB gain for parallel transitions compared with only 1.1 dB with distinct transitions), but with eight or more states, only trellis structures with distinct transitions are normally of interest, because parallel transitions limit the free ED gain to 3 dB.

The two better 8-PSK codes considered (4-state with parallel transitions and 8-state with distinct transitions) are simulated for the Gaussian channel and the BER performance is reported in [21, 56]. The performance of the coherent 4-state code with parallel transitions, and the coherent and differential 8-state code, all using a decoding depth of $D = 6\nu$, are presented in Figure 3.7. The lower bound asymptotic estimates for the coherent cases are also indicated, as obtained from equation (3.7).

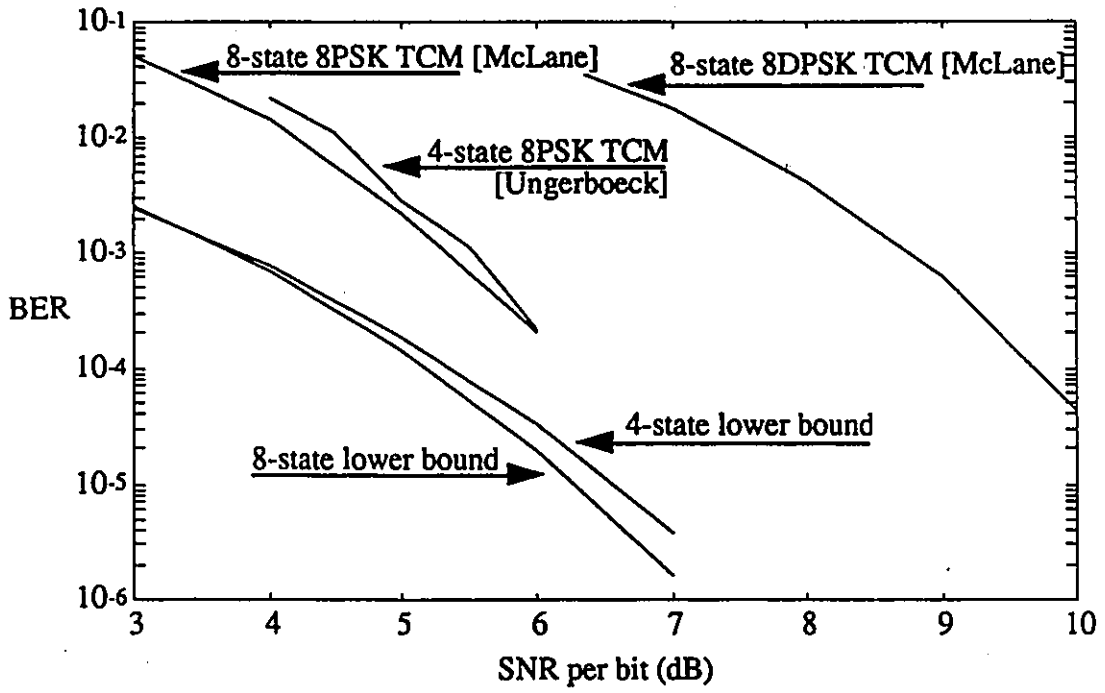

Figure 3.7: Published BER performance of coded 8-PSK schemes in AWGN channel.

States	$G_{8\text{-PSK}/4\text{-PSK}}$	$G_{16\text{-PSK}/8\text{-PSK}}$	$G_{4\text{-AM}/2\text{-AM}}$	$G_{8\text{-AM}/4\text{-AM}}$	$G_{16\text{-AM}/8\text{-AM}}$
4	3.01	3.54	2.55	3.31	3.52
8	3.60	4.01	3.01	3.77	3.97
16	4.13	4.44	3.42	4.18	4.39
32	4.59	5.13	4.15	4.91	5.11
64	5.01	5.33	4.47	5.23	5.44
128	5.17	5.33	5.05	5.81	6.02
256	5.75	5.51	5.30	5.81	6.02

Table 3.1: Free ED coding gains for TCM [56, 57].

Figure 3.8 indicates the advantage of trellis-coded modulation for the coherent and the differential signaling cases relative to QPSK. This advantage exists only for SNR values above a certain value, which is about 4 dB for the coherent case and 8 dB for differential. The coding gain increases for increasing SNR, up to its asymptotic limit.

Coding gains of up to 6 dB and more can be achieved, as shown in Table 3.1, where each coded scheme is compared to its uncoded counterpart (e.g. relative gain of coded 8-PSK over uncoded 4-PSK). Most of the coding gain (3 - 4 dB) is obtained with four or eight states. A higher number of states reduces the relative gain, i.e. achieving a 6dB gain requires a rather complex system.

Carrier phase tracking is a consideration with coherent systems. For 4- and 8-state coded 8-PSK systems, the SNR required to achieve a BER of 10^{-5} increases with increasing values of phase offset Δ_ϕ, until both systems fail at $\Delta_\phi = 22.5°$, even in the absence of noise. In contrast, uncoded 4-PSK requires a higher SNR at small phase offsets, but doesn't fail until $\Delta_\phi = 45°$ [57]. For 4-state 8-PSK, the use of a decision directed carrier phase loop that uses tentative decisions of the Viterbi algorithm is suggested for phase tracking [56].

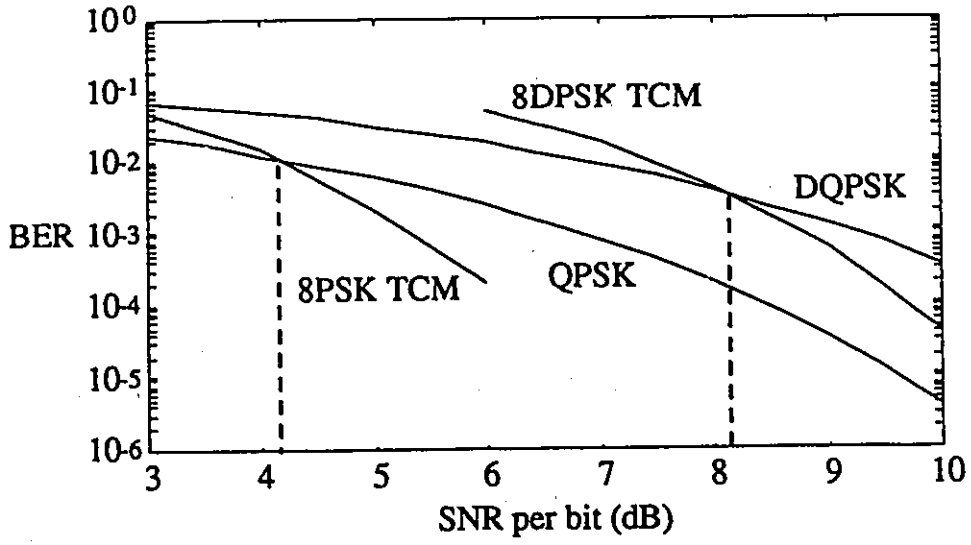

Figure 3.8: Comparison of the (D)QPSK and 8-(D)PSK TCM performances.

3.3.4 Using Differential Detection

Unlike for coherent detection, Euclidean distance is not the optimum decoding metric for differential detection to achieve the sequence closest to that transmitted. This is due to multiplication of two consecutive dispersive waveforms by the differential detector, so that the noise at the detector output is non-Gaussian and correlated [65].

However, coherent detection loses a great deal of its performance in environments where other kinds of disturbances are considerable, including multipath propagation, frequency selective fading, and phase noise, because the carrier recovery circuits start experiencing long acquisition times.

The use of I differential detectors, each of order $i = 1, 2, \ldots, I$ (where the i^{th} detector uses i unit delays), for metric computation in a soft-decision Viterbi decoder is found to improve the BER performance [65]. The decoder uses the detectors' unquantized outputs. This in effect introduces diversity in the system.

3.3.5 Optimization for Fading Channels

The minimum Euclidean distance criteria used by the Viterbi algorithm is optimum for TCM with the Gaussian channel, but not with the fading channel. Most studies though still use this sub-optimal metric because the optimal one is too complex.

When designing a trellis code for a fading channel, the effective code length (ECL) δ_H and the minimum product distance (PD) d_p become very important parameters [19, 66, 67, 68, 69]. They are defined as follows [19]:

δ_H : the minimum effective length taken over all error paths in the coded sequence set, where the effective length δ of an error path is the number of erroneous symbols on the error path, expressed as:

$$\delta = \sum_{i=0}^{\frac{M}{2}-1} w_i \tag{3.9}$$

where w_i represents the weight associated with the corresponding symbol distance Δ_i along the error path.

d_p : the minimum product distance taken over all paths with δ_H, where the product distance, denoted by $\underline{\Delta_p}$, is the product of the corresponding squared symbol distances along the error path and is given by:

$$\underline{\Delta_p} = \prod_{i=0}^{\frac{M}{2}-1} \Delta_i^{2w_i} \tag{3.10}$$

To minimize the probability of error, the code must be designed to maximize δ_H and d_p. Such codes may have a d_{free} that doesn't achieve its optimum value for the Gaussian channel, since this is not the design criteria [23, 66].

For codes with large δ_H, it is found that the probability of error is dominated by d_{free}, while for codes with small δ_H, the P_b is mostly dependent on δ_H , d_p and the number of erroneous bits on the error paths [19].

The codes optimized for the Gaussian channel, designed for a large d_{free} distance, achieve this distance over only a few branches in most cases. This proves detrimental on fading channels, where the distance should be spread more evenly over all the branches of a trellis path [68].

Rate $R_c = 2/3$, 8-PSK codes designed for the fading channel with side information (i.e. where the fading depth is known for each symbol interval) are presented in [68] for various number of states. Interestingly, the very short 8- and 16-state codes presented are the same as codes developed for the Gaussian channel. The advantage occurs for 32-states or more ($\nu \geq 5$) where these specially designed codes exhibit superior performance in fading channels, especially at high SNR values.

16-PSK codes designed using the above mentioned techniques show significantly improved BER and much lower error floors [19].

Finally, the BER performance of a TCM system is found to be much less sensitive to the decoding depth D in a fading channel (with no ISI) than it is in a Gaussian channel, which means that D can be chosen to be lower when used in a fading channel [21, 22, 69].

3.4 Equalization

The dispersion of the waveform, as mentioned previously, causes intersymbol interference. This can be reduced by the use of filters which act on the received signal to compensate for this interference. Such filters are called equalizers [26]. An equalizer is defined as being any device or signal processing algorithm that is designed to deal with intersymbol interference.

3.4.1 Linear Equalizer

The simplest filter is the linear, or transversal, equalizer, where the estimate $\hat{I}_k$ of the symbol at the k^{th} signaling interval is a weighted linear combination of the input signal sequence $\{v_{k-j}\}$:

$$\hat{I}_k = \sum_{j=-K}^{K} c_j v_{k-j} \tag{3.11}$$

where $\{c_j\}$ are the $(2K+1)$ tap weight coefficients of the equalizer filter, chosen to optimize a criterion such as peak distortion or mean square error (MSE). This optimization will determine the number of taps to use. The relative performance improvement due to the increase in the number of taps reduces as this value gets larger [11].

Another type of equalizer, the linear feedback equalizer, calculates $\hat{I}_k$ as a weighted linear combination of the input signal sequence $\{v_{k-n}\}$ in its feed-forward section where $n = (-K, \ldots, -1, 0)$, and the previous equalizer outputs $\{\hat{I}_{k-j}\}$ in its feedback section with $j = (1, 2, \ldots, K)$:

$$\hat{I}_k = \sum_{j=-K}^{0} c_j v_{k-j} + \sum_{j=1}^{K} c_j \hat{I}_{k-j} \tag{3.12}$$

This is not used in practice because its performance improvement over transversal equalization is small, and there is also a stability problem [26].

It is shown that a linear equalizer yields good performance on channels where the spectral characteristics are well behaved and do not exhibit spectral nulls. However, for channels with time-variant spectral characteristics that possess nulls, such as multipath radio channels, linear equalization is not well suited [26, 70]. Nonlinear equalization must therefore be considered.

3.4.2 Decision-Feedback Equalizer

The most common non-linear equalizer, the decision-feedback equalizer (DFE), has a feed-forward and a feedback section, and the symbol estimate is calculated as:

$$\hat{I}_k = \sum_{j=-K_1}^{0} c_j v_{k-j} + \sum_{j=1}^{K_2} c_j \bar{I}_{k-j} \tag{3.13}$$

where $\bar{I}_{k-m}$ represents previously detected symbols ($m = 1, 2, \ldots, K_2$); this imposes the non-linearity of the decision device. The tap coefficients $\{c_j\}$ are again chosen to optimize a criterion such as peak distortion or mean square error.

The feedback section results in the elimination of ISI from the previously detected symbols, provided that previous decisions are correct and that $K_2 \geq L$, where the discrete-time model of the channel is represented by an $(L+1)$-tap filter. The feed-forward section reduces the effect of ISI caused by symbols received following the symbol of interest.

Error propagation is caused by decision errors occurring in a DFE and propagating through the feedback section to increase the chances of making additional errors. The DFE is found to be better than the linear equalizer if the effect of error propagation is neglected [26]. It is shown in [70] that for a practical realization of a DFE in a slow fading channel application, the error propagation is negligible, thus one may assume that the DFE offers better BER performance than the linear equalizer for the indoor wireless channel, which has slow fading.

3.4.3 Calculation of Tap Weight Coefficients

Given that the minimum MSE criterion is used to optimize the linear equalizer's tap weight coefficients, the following equation must be solved [26, p.565]:

$$\vec{\Gamma}\mathbf{C} = \mathbf{S} \tag{3.14}$$

where $\mathbf{C} = (c_{-2}, c_{-1}, c_0, c_1, c_2)$ is the complex tap-weight coefficient vector, $\mathbf{S}$ is a column vector with elements s_l:

$$s_l = \begin{cases} f_{-l}^* & -L \leq l \leq 0 \\ 0 & \text{otherwise} \end{cases} \tag{3.15}$$

where $\{f_n\}$ are the equivalent channel tap weight coefficients, and the covariance matrix $\vec{\Gamma}$ is defined as:

$$\Gamma_{lj} = \begin{cases} x_{l-j} + N_0\delta_{lj} & |l-j| \leq L \\ 0 & \text{otherwise} \end{cases} \tag{3.16}$$

where δ_{lj} is the Dirac delta function, and x_{l-j} is the channel correlation, obtained from:

$$x_k = \sum_{n=0}^{L-k} f_n^* f_{n+k} \qquad k = 0, 1, 2, \ldots, L \tag{3.17}$$

3.4.4 Adaptive Equalization

Adaptive equalization is normally required for time-varying environments with unknown characteristics. In these situations, the tap weight coefficients $\{c_j\}$ are continuously adjusted on the basis of measurements of the channel characteristics. If the time variation of the channel is assumed to be slow compared to the information rate, then a part of the information can be used to track the time variations. A tutorial on adaptive equalization is presented in [71].

The equalizer coefficients $\{c_n\}$ can be calculated from knowledge of the channel coefficients $\{f_n\}$, but since this is not known in a time-varying channel, an alternate method is to use an iterative procedure such as the method of steepest descent. This algorithm is expressed at iteration step k in the form:

$$\hat{\mathbf{C}}_{\mathbf{k+1}} = \hat{\mathbf{C}} - \partial\hat{\mathbf{G}}_{\mathbf{k}} \tag{3.18}$$

where $\hat{\mathbf{G}}_{\mathbf{k}}$ is an estimate of the gradient vector $\mathbf{G}_{\mathbf{k}}$:

$$\mathbf{G}_{\mathbf{k}} = \vec{\Gamma}\mathbf{C}_{\mathbf{k}} - \mathbf{S} \tag{3.19}$$

$\hat{\mathbf{C}}$ is the estimate of the coefficient vector $\mathbf{C}$ and ∂ is the step-size parameter.

The convergence of the iterative process to obtain the coefficients is governed by the step-size parameter ∂. When using MSE as the optimization criterion, convergence is ensured if the following is satisfied:

$$0 < \partial < \frac{2}{\lambda_{max}} \tag{3.20}$$

where λ_{max} is the largest eigenvalue of $\vec{\Gamma}$, obtained from:

$$\lambda_{max} < (2K+1)(x_0 + N_0) \tag{3.21}$$

The convergence then depends on the number of taps $(2K+1)$, the auto-correlation x_0 of the channel obtained from equation (3.17), and the noise power density N_0.

3.4.5 Operation of the Equalizer in a Multipath Channel

When using an equalizer in a multipath propagation environment, an increase of the data symbol rate R_s (or the rms delay spread σ_T) causes a greater impact of the multipath channel on the received pulses, tending towards performance degradation due to ISI. At the same time, this increase in the multipath provides more internal diversity to the equalizer so the system tends towards performance improvement. Initially, performance improves with increasing data rate. This is due to the equalizer exploiting the increasing internal diversity of the received signal while ISI is negligible. For increased multipath impairment however, performance begins to decrease as the harmful effects of ISI become significant with respect to the gains due to the internal diversity [11].

The adaptive DFE applied to a fading channel is examined in [70, 72, 73, 74] using the MSE optimization criterion. A fundamental assumption made in those research works is that the system error probability is sufficiently low to assume that the received

symbols are correctly detected, which leads to negligible error propagation. The adaptive process uses the steepest descent or gradient algorithm, and doesn't depend on knowledge of source or noise statistics, or channel characteristics. The structure using feedback is found to be superior to the non-feedback structure for the MSE criterion. It is shown how performance in the equalized dispersive fading channel improves as the dispersion increases, because of the equalizer's enhanced implicit diversity, but worsens when the dispersion exceeds the equalizer's capability to mitigate the ISI by resolving the multipaths, as mentioned previously. The use of more taps in the equalizer increases the multipath handling capability. While mitigating ISI and additive noise, a receiver with a DFE also eliminates timing jitter and Doppler shifts [72].

3.4.6 Published Equalization Results

Theoretical adaptive transversal equalization using the MSE criterion with 4-QAM in indoor wireless communication is considered in [15] for bit rates R_b ranging from 1 to 64 Mbits/s. It is found that an outage probability of less than 10^{-3} for a BER no greater than 10^{-4} is achieved for rates up to 4 Mbits/s when affected by an rms delay spread σ_T of 25 ns, or up to 1 Mbit/s for 100 ns.

A BPSK IW system with a DFE having three feed-forward ($K_1 = 2$) and three feedback taps ($K_2 = 3$) can handle data rates one order of magnitude higher than a system without equalizer [6]. Similar results for BPSK with a DFE are found in [7].

A study of QPSK with DFE in [11] shows a performance degradation for increasing rms delay spread values when equalization is not used, and an increase in performance when the DFE is used, within a certain limit. For a 7-tap DFE with SNR = 30 dB, a system transmitting at $R_b = 10$ Mbits/s will see its BER reduced as σ_T is increased up to 200 ns, beyond which the BER performance drops sharply.

3.4.7 Non-Coherent Signaling with Adaptive Decision-Feedback Equalization

The use of an adaptive DFE almost precludes non-coherent signaling, as previously detected symbols $\tilde{I}_{k-m}$ $(m = 1, 2, \ldots, K_2)$ are required to obtain the symbol estimate $\hat{I}_k$, and this means that the differential detection for non-coherent signaling must be placed between the equalization and the decision device, where it will add more non-linearity to the tap weight coefficient algorithm. This is not looked at any further as it would stray from the work's goal, though it would be interesting for further research.

Thus coherent signaling is required when using an adaptive DFE as described in the literature, otherwise the algorithm to calculate $\{c_j\}$ must be redesigned for the extra non-linearity.

3.4.8 Adaptive Equalization with Trellis Coding

The use of adaptive equalization with trellis-coded signals further complicates things, because of the delay inherent in the Viterbi decoding of the signals [26, pp.600-601].

One possible technique to compensate for this delay is to have the equalizer make a decision at its output, independently of the Viterbi decoder, to obtain an estimate of the error signal required by the adaptive algorithm. These estimated decisions are generally unreliable and cause a degradation in the operation of the equalizer, thereby reducing the reliability of the final decoder decisions.

Alternatively, the post-decoding decisions from the Viterbi decoder are used to obtain the error signal. This is reliable when using a linear equalizer, where the decoding delay is easily overcome, as explained in [75]. In cases where the DFE is used, reliable decisions are required for the feedback section, and a conventional DFE cannot accommodate the decoding delay, as the linear equalizer can; a predictive DFE [26] with a

periodic interleaver/de-interleaver pair is required. This technique is described for the Gaussian channel in [76] and for the fading multipath channel in [77].

3.4.9 Use of Fractionally-Spaced Filters

All equalizers mentioned employ a T_s-spaced filter for the feed-forward section. This is only good for systems that have a matched receive filter with optimum sampling. The channel response is generally not known so an ideal matched filter cannot be designed. For this reason, a fractionally-spaced feed-forward filter is used in practice to eliminate system sensitivity to timing error. The feedback filter taps remain spaced at T_s.

3.5 Recent Developments

Recent developments to solve intersymbol interference problems in TCM systems have seen the equalizer replaced in favour of a modified adaptive trellis using different methods, such as Reduced-State Sequence Estimation (RSSE) [78, 79], Delayed Decision-Feedback Sequence Estimation (DDFSE) [80], and others [81]. This is beyond this scope of the study and is only mentioned here for completeness.

3.6 Summary

Trellis-coded modulation and equalization techniques are presented as potential methods to reduce the effect of the indoor wireless channel on the transmitted information.

Trellis-coded modulation is explained, and details of such code's design are mentioned for the cases of the Gaussian and the fading channels. A brief presentation is given of the Viterbi algorithm using the Euclidean distance as the decision metric. Though this is seen to be a sub-optimal metric for fading multipath channels, it is chosen for its simplicity and ease of implementation.

The three trellis codes suggested for use are designed for the Gaussian channel, and offer coding gains of up to 3.6 dB. Some published simulated BER results for these codes are given. It is mentioned that the optimal 8-state code designed for the Gaussian channel is also optimal for the fading channel.

The decoding depth is chosen as $D = 6\nu$ to achieve negligible truncation error with minimum decoding delay. The use of non-coherent signaling is seen to reduce the optimality of the Euclidean distance metric for Gaussian channels, and also increase the effect of the spreading caused by the channel, but it is chosen to avoid recovery problems encountered in fading multipath channels.

The equalizer is used to reduce the effect of ISI caused by the dispersive IW channel. The linear form is shown to be inadequate with a channel that possesses spectral nulls, so decision-feedback equalization is recommended for the time-varying IW case. The non-linear DFE is seen to possess implicit diversity that permits it to mitigate signal dispersion for a certain range of rms delay spread, beyond which it can no longer resolve the multipaths. Coherent signaling should be used with a DFE, to avoid the non-linearity of the differential detector.

Chapter 4

Simulation System Setup

This chapter describes how the system simulations are conducted, and an overview of the simulation platform and tools is presented.

Firstly, in Section 4.1 the system implementation is described, and basic system considerations are given. The different system components are explained in Section 4.2, including the indoor wireless channel, the QPSK and TCM modulators and demodulators, and the equalizer. BER performance results for the Gaussian channel, as obtained through simulations, are also presented to justify the working condition of the systems. A brief explanation of BOSS [82], the simulation package used to develop the systems and execute the simulations on a bit-by-bit basis, is presented in Section 4.3, with a description of some of the most important simulation parameters. Finally, the geometric mean is presented in Section 4.4 as the measure of choice to represent the simulation results.

4.1 System Implementation Considerations

A low-pass equivalent system is used in the simulations to avoid excessive processing times. The channel considered is not band-limited, transmit and receive filters are not used, and there is no pulse shaping. Perfect signal synchronization is considered for the

sampling, so there is no timing jitter. Information about the phase distortion due to the channel is considered unknown, thus non-coherent signaling is used. This is assumed since for fading channels, obtaining the carrier reference signal for coherent detection can be difficult, especially during fades. The channel impulse response is fixed for the duration of the simulation, and an ensemble averaging is done over the fixed impulse responses to assess the general performance of the time-varying impulse response, where it is assumed that the fixed impulse responses are sufficiently representative snapshots of the time-varying impulse response. The frequency of operation f_c is taken as 1.5 GHz because the channel model parameters from [24] are obtained for this operating point. The data rate R_b considered is 10 Mbits/s. Only intersymbol interference caused by the multipath channel is considered as interference source (i.e. no other interferers or users exist).

4.2 System Setup

The general system, shown in Figure 4.1, contains the data source, the modulator, the channel, the equalizer, and the demodulator. For performance results, the demodulated data is compared bit-by-bit with the original data at the modulator input to observe and count errors. Each of these system modules are now described.

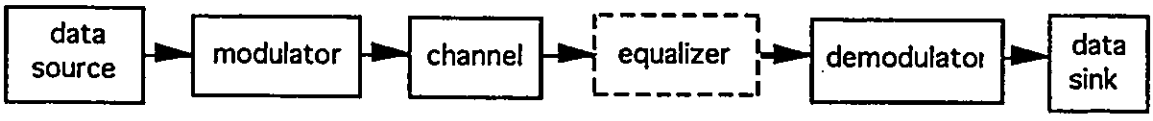

Figure 4.1: General system block diagram.

4.2.1 Data Source

The data source is a simple random bit stream generator, where both outputs are equiprobable. The underlying distribution is uniform over the interval [0,1), with a decision threshold of 0.5.

4.2.2 Channel

The IW channel impulse response is generated from the model in [24] using the following parameters:

α	γ (ns)	Γ (ns)	$1/\lambda$ (ns)	$1/\Lambda$ (ns)	G_t	G_r	λ_c (m)	r (m)
3.5	20	60	5	300	1.0	1.0	0.2	10

As discussed below (Table 4.1), the choice of α, G_t, G_r and r seems to have little impact on the statistics of the impulse response. The value r is chosen as 10m to represent a probable maximum distance between receiving and transmitting antennas for a micro-cellular network. The distance-power law exponent α is chosen arbitrarily as 3.5, as are the values of G_t and G_r.

A maximum of six clusters are generated with no more than 500 rays in each cluster. The transmission delay is fixed at zero by having the first ray of the first cluster occur at time $t = 0$ ns. To avoid huge impulse response data files, all rays more than 60 dB below the ray at time $t = 0$ ns are truncated. This truncation is justified below.

An ensemble of one hundred distinct channel impulse responses are generated for simulation purposes. Since it characterizes the impulse response, the rms delay spread σ_T for each file is calculated. The impulse responses are then classified by ranges of rms delay spread, i.e. $\sigma_T = (20,25], (25,30], \ldots, (75,80]$ ns. This is convenient when classifying the simulations' performance results.

Set	α	G_t	G_r	r (m)	min σ_T (ns)	mean σ_T (ns)	median σ_T (ns)	max σ_T (ns)
1	3.5	1.0	1.0	10.0	10.9	38.2	37.1	105.1
2	3.0	1.6	1.6	10.0	8.9	37.8	36.0	95.6
3	3.0	1.6	1.6	5.0	7.6	38.0	36.5	100.5
4	3.0	1.6	1.6	2.0	8.9	36.8	34.3	100.8

Table 4.1: RMS delay spread statistics for impulse response ensembles.

To get a precise distribution of σ_T, a set of 2000 impulse responses is generated for purposes of calculating the rms delay spread statistics only. Since some of the model parameters used for the simulation impulse responses are different than those in [24], more sets of 2000 impulse responses are generated for various combinations of parameter values and their σ_T statistics calculated. The mean rms delay spread values and other σ_T statistics are given in Table 4.1 for the sets of 2000 impulse responses, and their distributions are as shown in Figure 4.2, represented by solid lines. As these are almost identical, no effort is made to identify them individually. It can be seen from Table 4.1 that the mean value is not affected much by the changes in parameters, and the distributions are almost identical. The dotted line is obtained from the initial 100 impulse responses used for simulations. This set is less representative because of the smaller sample size. These statistics obtained from the model compare with a median of 25 ns and a maximum of 50 ns obtained in [24] from the measurements used to develop the model. The discrepancy in these results is not important for the present study, which is more interested in the system performance as a function of the rms delay spread σ_T than with the rms delay spread distribution.

Calculations are done to evaluate the effect of truncation on the impulse response. The rms delay spread values of the one hundred impulse responses ensemble are found to vary by less that 0.1% with an increase in the truncation floor from 100 dB to 60

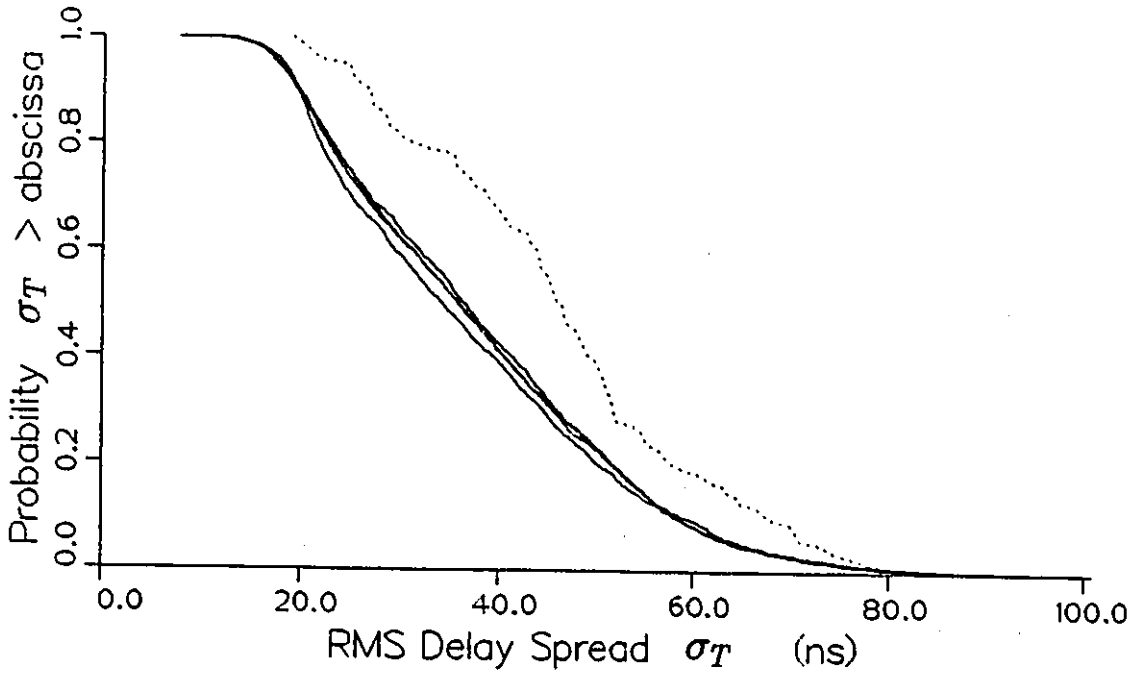

Figure 4.2: RMS delay spread ensemble distributions.

dB, so the impulse response is assumed to be practically unaffected by this truncation, as pertaining to its effect on the transmitted signal.

Typical impulse responses are shown in Figures 4.3, 4.4 and 4.5, where the ray amplitudes are normalized only for these Figures with respect to the maximum ray amplitude, which is not necessarily the first ray. The first response shown has $\sigma_T = 19.2$ ns, which is near the minimum, the second has $\sigma_T = 38.8$ ns, close to the average, while the last figure shows an impulse response with $\sigma_T = 79.6$ ns, which is near the maximum. The effect of increasing the rms delay spread is noticed with significant rays occurring further from zero, which is an indication of the dispersiveness of the channel.

To reduce the simulation to a bit-by-bit process, the IW channel impulse response is modeled as an equivalent tapped delay-line with symbol-period delays and complex tap weight coefficients $\{f_n\}$, as shown in Figure 4.6, with additive white Gaussian

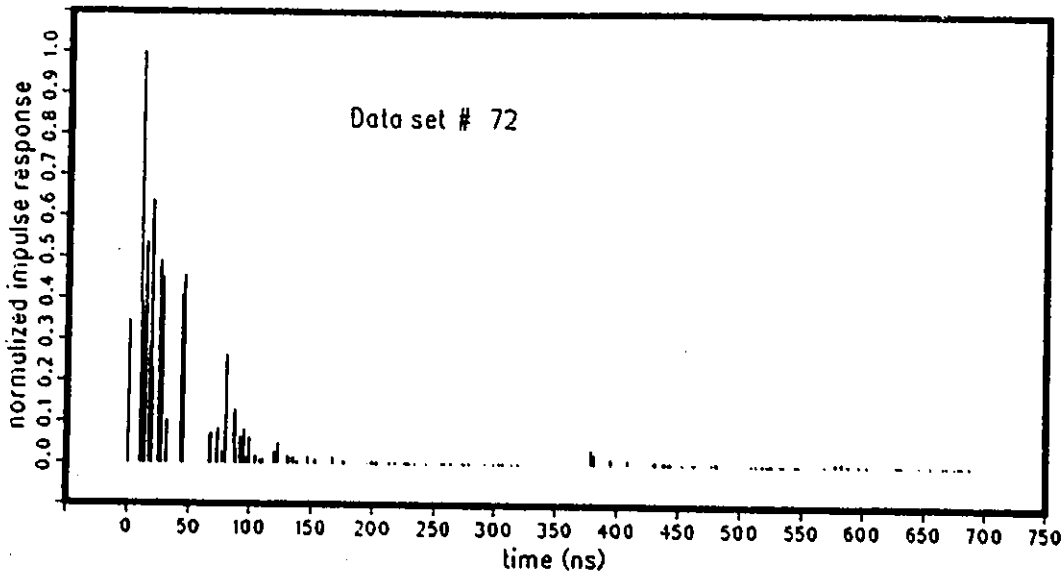

Figure 4.3: Normalized channel impulse response with $\sigma_T = 19.2$ ns.

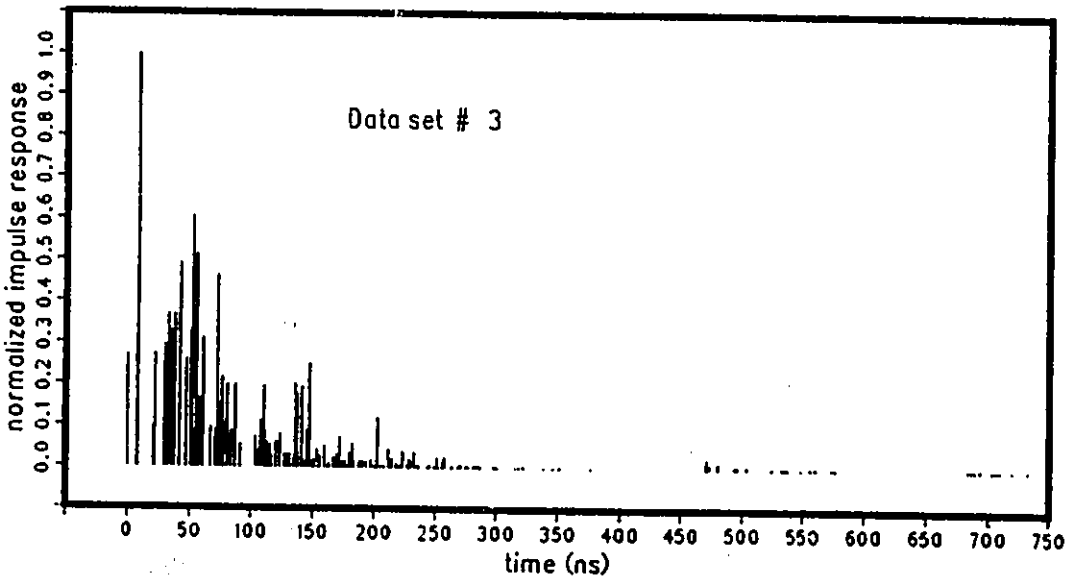

Figure 4.4: Normalized channel impulse response with $\sigma_T = 38.8$ ns.

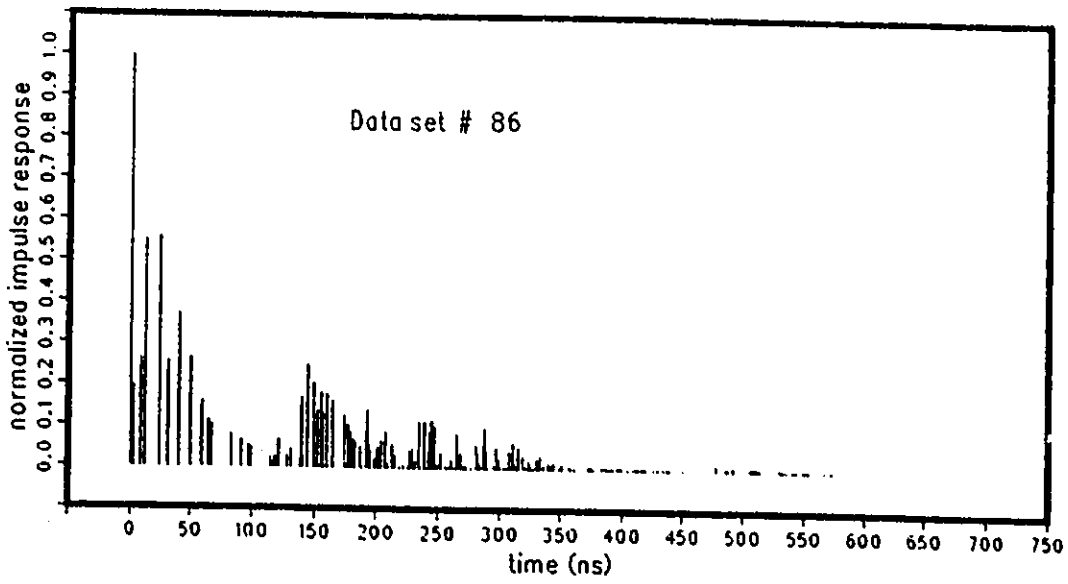

Figure 4.5: Normalized channel impulse response with $\sigma_T = 79.6$ ns.

noise. Assuming that sampling occurs at the symbol mid-point, the complex tap weight coefficients are calculated as follows for $R_b = 10$ Mbits/s, where the symbol period is $T_s = 200$ ns for QPSK and 8-PSK TCM: all rays occurring between 0 and 100 ns affect the present symbol and are summed vectorially to obtain the equivalent resulting ray f_0 which represents the effect of all these rays on this symbol; all rays between 100 and 300 ns affect the previous symbol and are summed vectorially to get f_1; and so on for rays between 300–500ns, 500–700 ns, ... This is represented by Figure 4.7. For other data rates, the equivalent channel is obtained similarly except that the summation ranges must be scaled to take into account the respective symbol period.

The SNR as used in the simulation to calculate the power of the AWGN is defined as follows:

$$\text{SNR} = 10 \log \frac{E_s}{N_o} \tag{4.1}$$

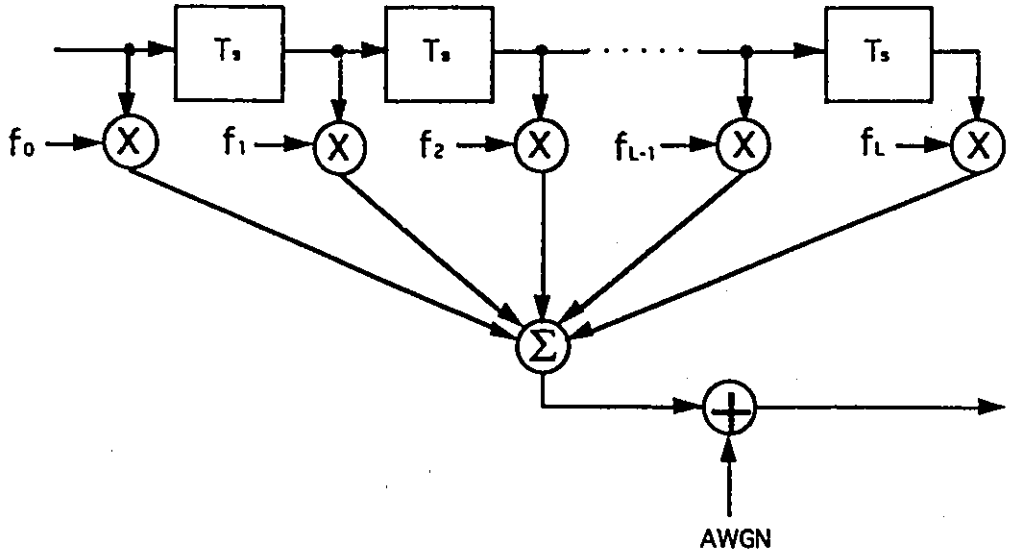

Figure 4.6: Tapped-delay line model of the indoor wireless channel.

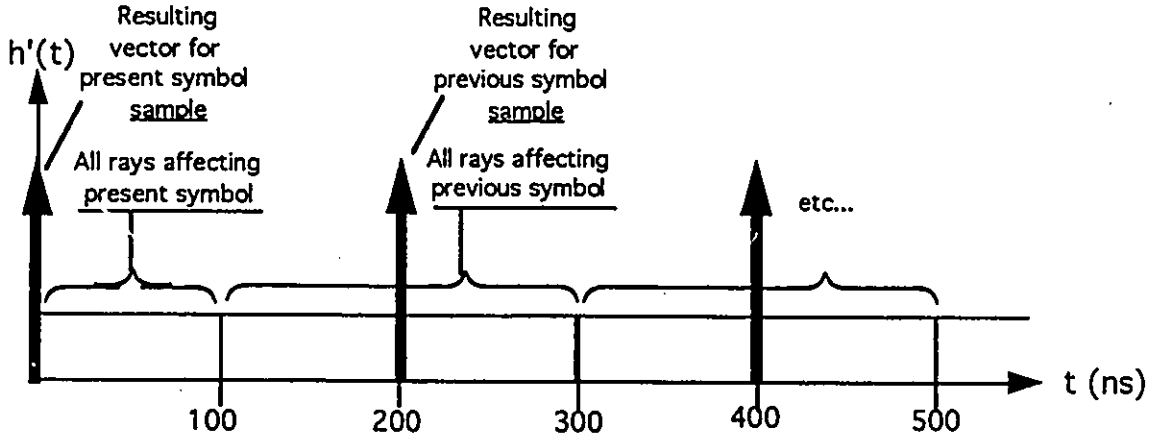

Figure 4.7: Reduction of the channel impulse response to equivalent rays per symbol.

where E_s is the signal energy per symbol at the receiver, that is:

$$E_s = E_{PSK} \sum_{l=0}^{L} f_l^2 \tag{4.2}$$

E_{PSK} is the energy transmitted per symbol to the channel input and f = $(f_0, f_1, \ldots, f_L)$ represents the equivalent complex channel tap weight coefficient vector. This measure of SNR could be called signal plus interference to noise ratio (S+I)/N, but it is not used to avoid confusion with the more common signal to interference plus noise ratio S/(I+N) measure commonly referred to as SINR.

4.2.3 QPSK System

The modulator and demodulator sections of the QPSK system are shown in Figures 4.8 and 4.9 respectively. The mapper takes the input 2-bit symbol and maps it onto one of four phase signals using the Gray code. The differential encoder and detector are given in Figures 4.10 and 4.11 respectively, where ( )* represents the complex conjugate function, and T_s is the symbol period.

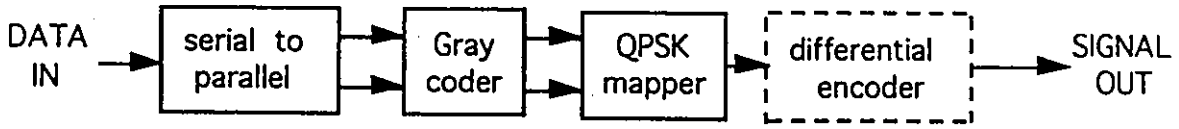

Figure 4.8: Block diagram of the (D)QPSK modulator.

Simulations are executed for the QPSK and DQPSK systems on the Gaussian channel, and the results given in Figure 4.12 indicate that the performance corresponds to the theoretical curves as given by equations (3.2) and (3.4), so both systems are properly calibrated.

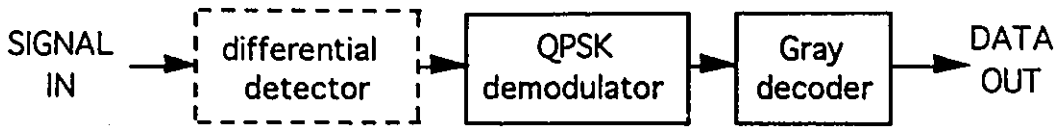

Figure 4.9: Block diagram of the (D)QPSK demodulator.

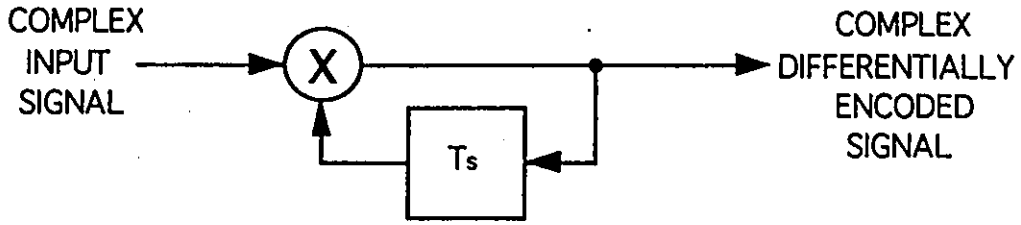

Figure 4.10: Block diagram of the differential encoder.

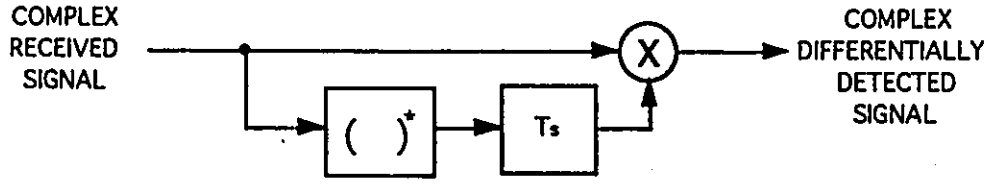

Figure 4.11: Block diagram of the differential detector.

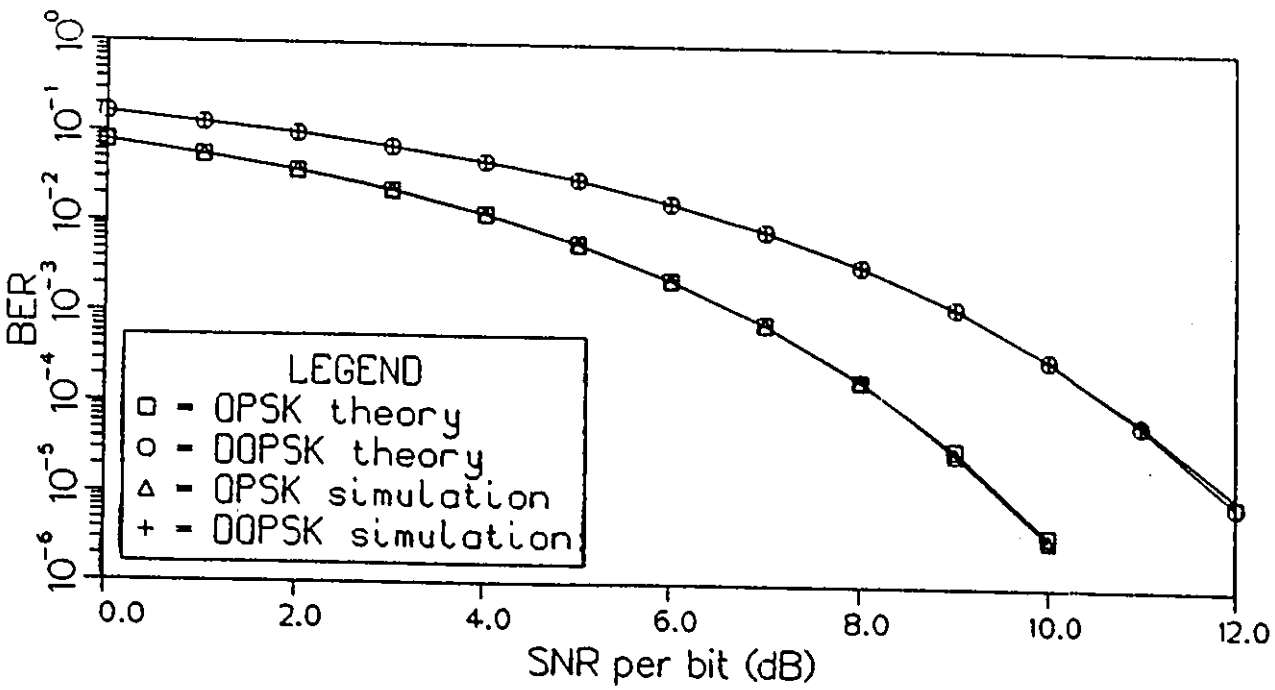

Figure 4.12: Performance of (D)QPSK in the Gaussian channel.

4.2.4 TCM System

The modulator and demodulator sections of the TCM system are shown in Figures 4.13 and 4.14 respectively. The differential encoder and detector are as given previously in Figures 4.10 and 4.11. The 8-PSK mapper simply maps the 3-bit symbol input onto one of eight phase signals.

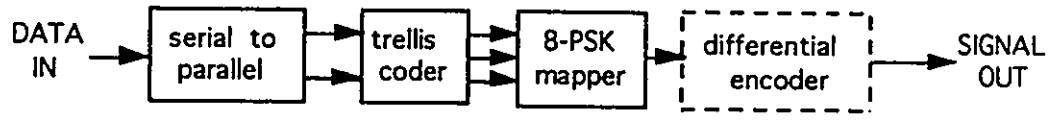

Figure 4.13: Block diagram of the TCM modulator.

The rate $R_c = 2/3$ convolutional trellis encoders used are given in Figures 4.15, 4.16 and 4.17 for the 4-state code with parallel transitions, the 4-state code with distinct

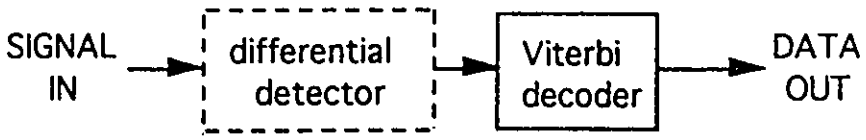

Figure 4.14: Block diagram of the TCM demodulator.

transitions, and the 8-state code with distinct transitions, respectively. These three codes are presented in Section 3.3.3, with their trellis structure diagrams given in Figures 3.4, 3.5 and 3.6 respectively.

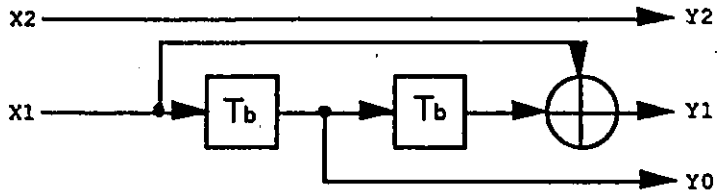

Figure 4.15: Encoder structure for the 4-state code with parallel transitions.

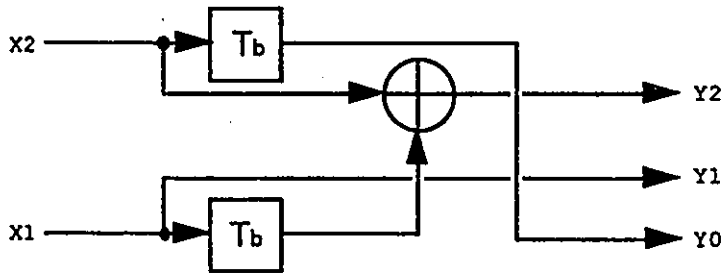

Figure 4.16: Encoder structure for the 4-state code with distinct transitions.

The Viterbi algorithm uses the code's trellis structure to decode the information, so three different algorithms are developed. The metric used is the minimum Euclidean

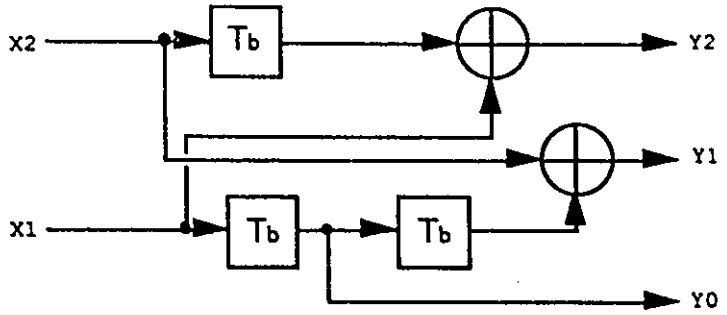

Figure 4.17: Encoder structure for the 8-state code with distinct transitions.

distance. This metric is optimum for coherent signaling with the Gaussian channel, but not for non-coherent signaling or fading channels; however, it is chosen because of its simplicity and its ease of implementation.

The three codes are simulated on the Gaussian channel with coherent and differential signaling using a decoding depth $D = 6\nu$, and performance results are shown in Figure 4.18, where coherent signaling using the 4-state code with distinct transitions is identified as C4D, differential (or non-coherent) signaling using the 4-state code with parallel transitions as D4P, and so on. Simulation results obtained are identified as *"sim"*, and *"McL"* represents previously mentioned simulation results taken from reference [21]. Those published simulation results coincide with the simulation results obtained, so the TCM system is judged to be properly calibrated. There is no advantage to using the 4-state code with distinct transitions in the Gaussian channel, as its BER performance is, as shown in Figure 4.18, worse than that for the other two TCM codes. For this reason, it will not be used in any further simulations with the assumption that it cannot outperform the other codes (4- and 8-state), even on dispersive channels.

Simulations are executed using the 4-state code with parallel transitions to examine

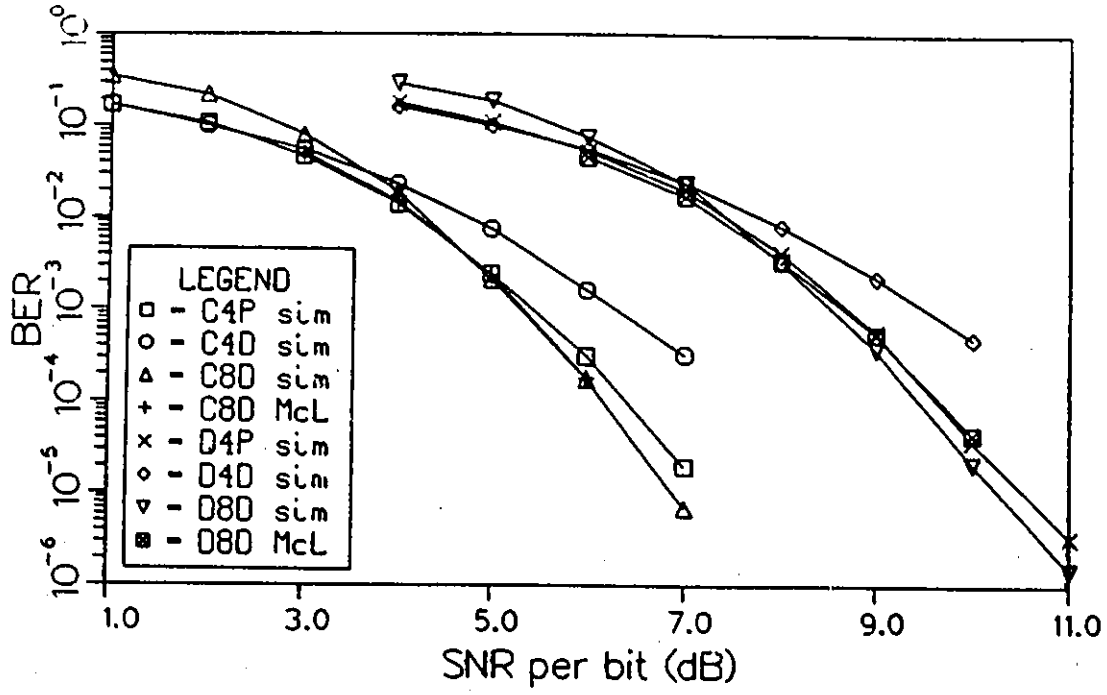

Figure 4.18: Performance of TCM in the Gaussian channel.

the effect of the decoding depth on the system performance. Both the coherent and the differential cases are considered for $D = 4\nu$ (8 symbols), 6ν (12 symbols), 9ν (18 symbols) and 25ν (50 symbols). Results as shown in Figure 4.19 indicate that there is no significant improvement beyond a decoding depth of 9ν. As no other simulation was done for values between 6ν and 9ν, it is impossible to see beyond which point between these values there is really no negligible improvement.

The decoding depth D chosen for all subsequent simulations is six times the constraint length of the code ($D = 6\nu$), as suggested in the literature (see Section 2.3.2); for the 4-state code, this represents $D = 12$ symbols, and for the 8-state code, $D = 18$ symbols.

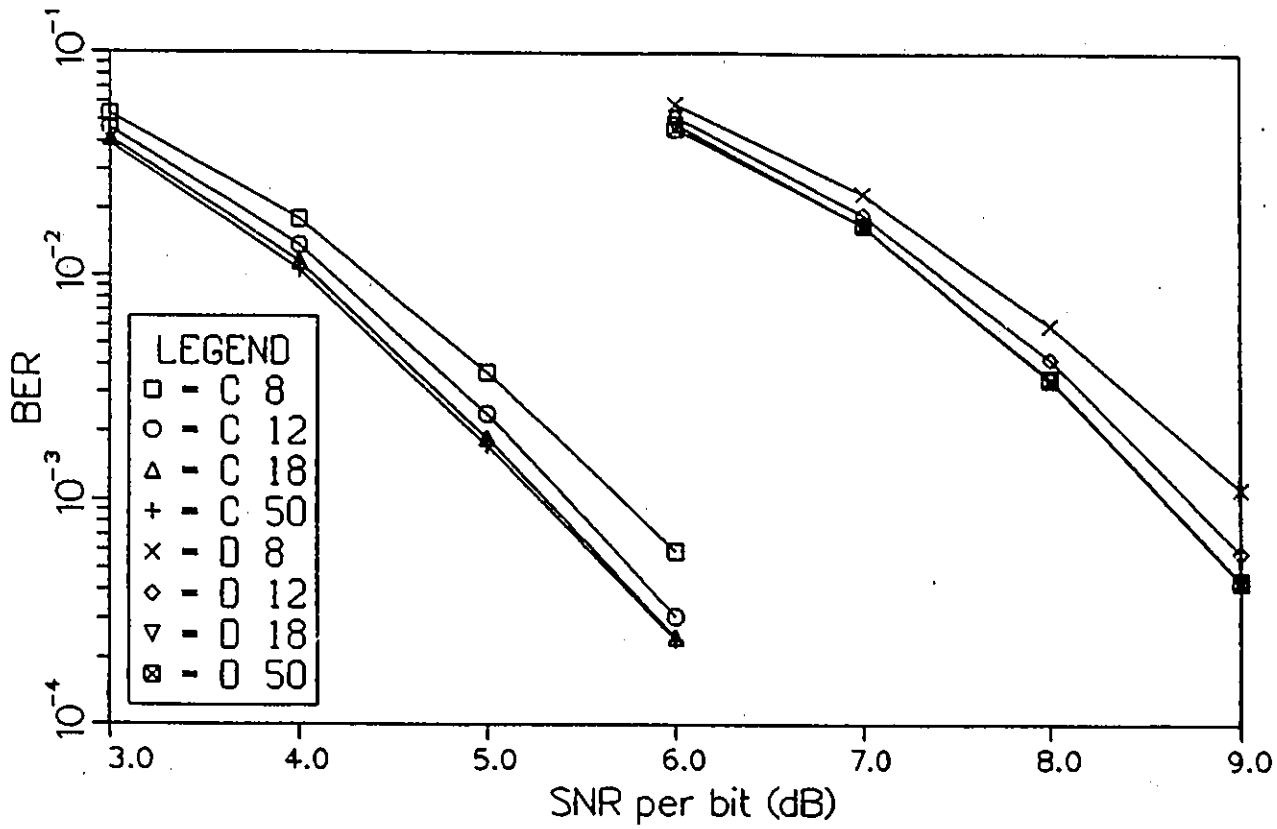

Figure 4.19: Effect of the decoding depth on TCM performance.

4.2.5 Equalization

For purposes of equalization, first a simple fixed-tap linear equalizer is used with DQPSK as well as the 4- and 8-state TCM schemes. The structure used is as shown in Figure 4.20. It is used in 5-tap and 3-tap configurations, with coefficients $c_{-2} = c_2 = 0$ for the latter case. Sampling in the simulations is made to be optimal, so all equalizers considered use T_s-spaced taps.

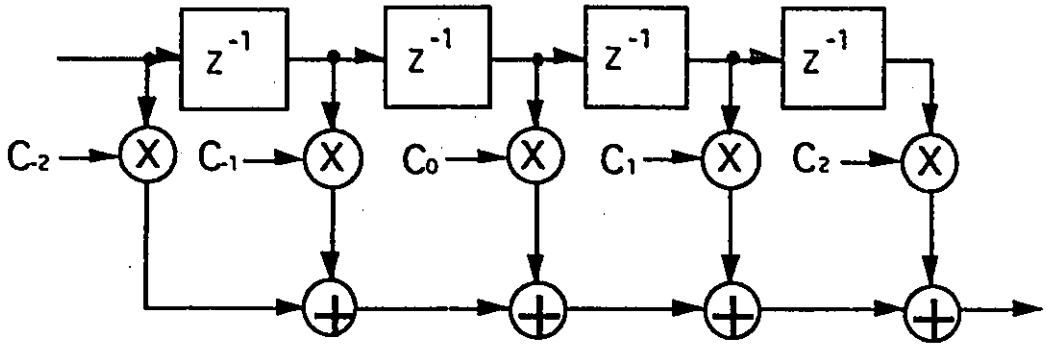

Figure 4.20: Fixed-tap linear equalizer structure with 5 taps.

The filter tap weight coefficients are calculated from theory using the MSE criterion by solving:

$$\vec{\Gamma}\mathbf{C} = \mathbf{S} \tag{4.3}$$

as explained in Section 2.4.3. The c_0's obtained are on the order of 10^3 to 10^4, which is reasonable given that the first channel tap f_0 varies around 10^{-3} to 10^{-4}.

It is shown in the next chapter that, though $\mathbf{C}$ is a function of N_o, approximating $\mathbf{C}$ by ignoring this value changes very little in the performance for the range of SNR considered, and most importantly facilitates the simulations.

It is interesting from a theoretical point of view to note that the equivalent equalized

channel, which is the result of the convolution between the channel with taps $\{f_j\}$ and the equalizer with taps $\{c_n\}$, obtained as:

$$y_n = \sum_{j=-\infty}^{\infty} f_j c_{n-j} \tag{4.4}$$

gives an equivalent response where the phase of y_0, the present symbol tap, is 0° for a 3-tap equalizer, and 180° for a 5-tap configuration. This indicates that the equalizer, in its theoretical form with fixed taps, can compensate for the channel phase shift even when it is unknown. This could be used to advantage by coherent signaling systems without requiring carrier phase recovery circuits. This is only mentioned here briefly, as it corresponds to a very simplified theoretical situation and may have no practical equivalent.

An adaptive MSE linear equalizer in a 3-tap configuration used with DQPSK only is also considered for comparison with the fixed-tap linear equalizer. It is implemented as shown in Figure 4.21, and has the differential detector and the Gray decoder after the decision device. The QPSK constellation remains unchanged by the differential detection, so this practice is deemed acceptable, especially in view of the results as given in the next chapter. This construction is necessary given that introducing the differential detector before the decision device introduces a non-linearity in the equalizer, which is undesirable and thus should be avoided.

The parameter ∂ indicated in Figure 4.21 is a positive number, but it must be small enough to ensure that the iterative process for the adaptive equalizer converges. As shown in Section 2.4.4, the convergence depends on the number of taps $(2K + 1)$, the sampled auto-correlation element x_0 of the channel, and the noise power density N_0.

Calculations of the step-size ∂ for the 3-tap equalizer with SNR = 4 to 10 dB indicate that its value lies in the range of 10^6 to 10^8 for the set of 100 impulse responses used

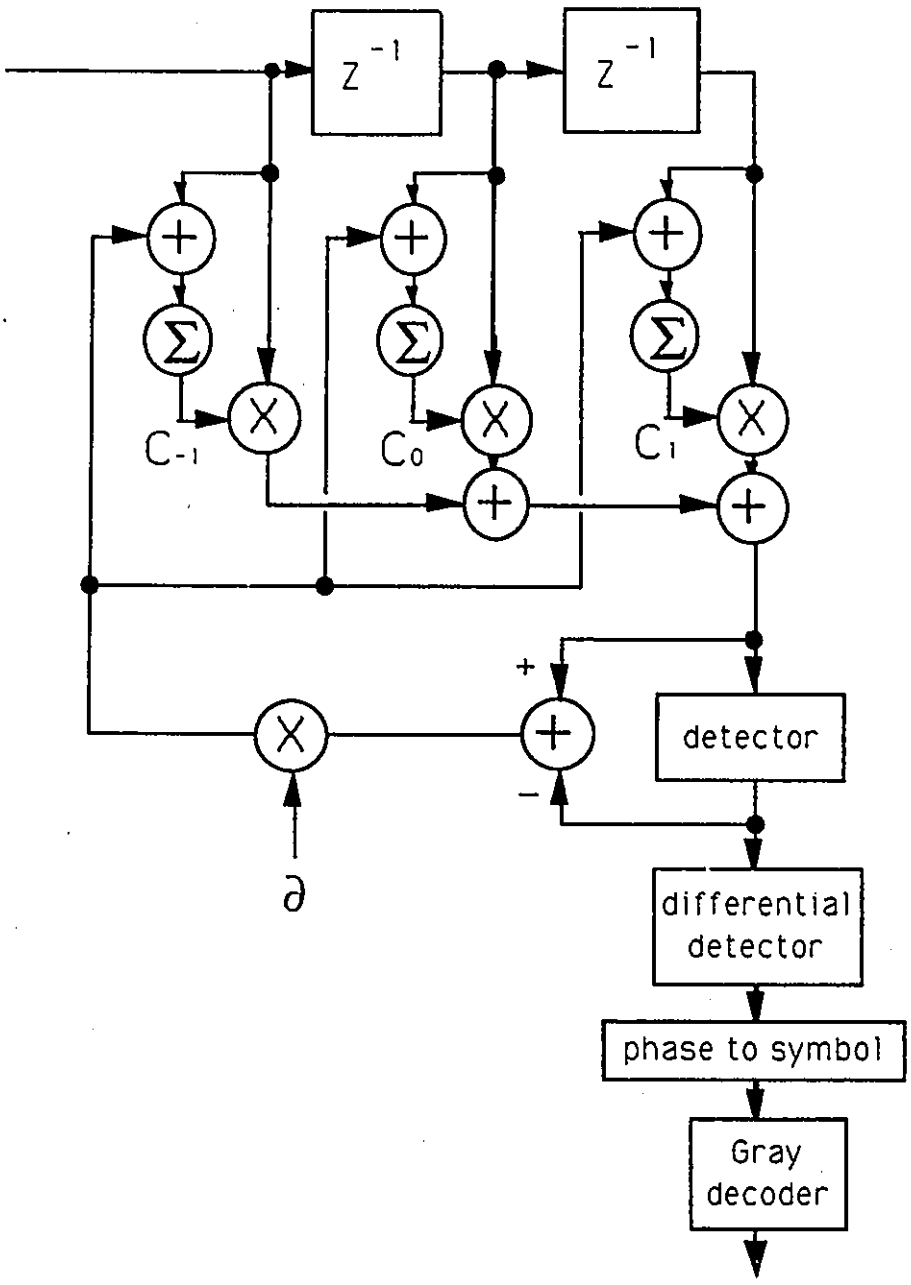

Figure 4.21: 3-tap adaptive linear equalizer with DQPSK demodulator.

for the simulations. Such large values can cause convergence problems. The simulation system as set up is rather sensitive to this parameter, so considerable attention is spent to find a proper value that will optimize the performance results.

The adaptive linear equalizer is not applied to the TCM system, nor is the DFE used in any of the simulations. These are considered to be beyond the scope of this study, especially considering the computer execution time factor, but it is known that the DFE easily outperforms the linear equalizer for BER values below about 10^{-3} [26]; therefore, given any results obtained with the linear equalizer, one can extrapolate better performance with the DFE.

4.3 Overview of Simulation Software and Parameters

The simulation application package used, BOSS [82] (which stands for Block Oriented System Simulator), provides the user with a complete interactive environment for simulation-based analysis and design of any system which can be represented in block diagram form, where each block performs signal processing operations. Time-domain simulations of these systems can be performed, and the supplied library database contains functional blocks most suitable for communication systems simulation, though others can easily be developed using a hierarchical block diagram approach or user-written FORTRAN code.

An important aspect of the BOSS application is its powerful post-processor and graphical interface, which permits signal output in various formats, including time-domain and frequency-domain.

The important simulation parameters for the systems developed for this study include:

- **DT**: Simulation step in seconds (not real time), chosen as 0.5×10^{-7} (or 1/2 bit period) for $R_b = 10$ Mbits/s. The signals in the simulated system are updated every DT time step. This chosen value constitutes the upper limit due to delays in the system. No lower limit exists, however smaller time step values increase the simulation execution time. If the study were to include spectral considerations, such as pulse shaping, or transmit and receive filters, the simulation time step required would be chosen to satisfy the Nyquist sampling criterion accordingly. This is not the case for the present study, where only two samples per bit are sufficient.

- **S-T**: The simulation stop time in seconds (again not in real time). It is chosen as 1.0 second for this study, which means that 10 Mbits pass through the system for $R_b = 10$ Mbits/s during the simulation, unless the execution is halted prematurely. This value is chosen to keep processing time down while achieving BER performance results over an interesting range.

- **MAXERR**: The maximum number of bit errors permitted to occur at the demodulator output before the execution is prematurely terminated. This is useful to avoid unnecessarily long processing times. This value was originally set at 2000, which means that the simulation executes until 2000 errors are accumulated, or until 1.0 second has elapsed, whichever occurs first. It was realized only near the end of the simulation work that even 100 accumulated errors are sufficient to give a representative result, therefore most simulations used MAXERR of 2000 and 500. For the equalizer simulations, the parameter MAXERR was set to 100.

Simulations were executed to obtain the BER performance of DQPSK and TCM

over the IW channel for various SNR with and without equalizer. Results for these are given in the next chapter.

4.4 Interpretation of Performance Results

Once the simulation results are obtained for all the desired situations, they must be properly treated to obtain a representative indication of performance. Because of the slow fading characteristic of the IW channel, performance analysis is accomplished under a quasi-stationary assumption, i.e. given the performance for a stationary channel, the average is taken over the channel ensemble statistics.

To obtain the BER performance of a system as a function of the rms delay spread σ_T for a specific SNR, a representative average result must be obtained from the simulation results for each individual rms delay spread ranges chosen. This should give a representation of the performance in a time-varying channel for the whole rms delay spread range.

The general method normally used to obtain a representative value is the arithmetic mean. However in this situation, another measure is called for. The geometric mean is recommended when a few of the elements in the sample have values that are much larger than most [83], as is often the case for BER results, which can typically vary over a few orders of magnitude. These larger values influence the geometric mean less than the arithmetic mean, so it is more appropriate as a representative value.

The geometric mean is defined as the n^{th} root of the product of all numbers, given n positive numbers:

$$\bar{x}_G = (x_1 \times x_2 \times \ldots \times x_n)^{1/n} \qquad x_i > 0 \tag{4.5}$$

which is equivalent to:

$$\log \overline{x_G} = \frac{1}{n} \sum_{i=1}^{n} \log x_i \tag{4.6}$$

This is the typical measure used to represent the obtained results. Thus for a measure of performance as a function of the rms delay spread, the geometric mean is obtained for the BER results of each individual rms delay spread range, given the SNR. Otherwise, for an overall measure of performance as a function of the SNR, the geometric mean is taken over all simulation results regardless of the rms delay spread, given a certain SNR.

4.5 Summary

The systems as used for the simulations are given and preliminary results with the Gaussian channel indicate that both the QPSK and TCM systems are properly calibrated.

Only two TCM codes are considered for further simulation: the 4-state code with parallel transitions and the 8-state code. A decoding depth of $D = 6\nu$, as recommended in the literature, is used for all subsequent simulation of the TCM system.

The linear equalizer is presented in its fixed-coefficient and adaptive forms, both of which are used with the IW channel systems. All taps are T_s-spaced because sampling in the simulation is made optimum. The adaptive equalizer with TCM, and the decision-feedback equalizer are not considered because of their implementation complexity and time limitations.

The BOSS simulation package used is very briefly described, and the geometric mean is presented as the representative measure of choice for the BER simulation results.

Chapter 5

Results and Discussion

This chapter presents the performance results obtained from computer simulations for the various TCM codes considered with the indoor wireless channel.

The simulation results are compiled and presented in graph form to simplify the presentation. When there is a need to compare different configurations, the relevant figures are presented with the same scale to ease comparisons. The results presented are for the DQPSK and differential 8-PSK TCM systems with a data rate of R_b = 10Mbits/s using the dispersive indoor wireless channel, firstly without equalizer in Section 5.1, and then with equalizer in Section 5.2. All simulations with TCM use a decoding depth of $D = 6\nu$. A preliminary version of these results is presented in [84].

5.1 Performance over the Dispersive Indoor Wireless Channel

Bit error rate performance results for DQPSK and the 4- and 8-state differential 8-PSK TCM schemes are presented in Figures 5.1, 5.2 and 5.3 respectively, where each curve is identified as the BER performance versus the rms delay spread σ_T for a given SNR of 4, 6, 8, 10 or 12 dB. The TCM codes used are obtained from the encoders in Figures 4.15 and 4.17 with the trellis shown in Figures 3.4 and 3.6 for the 4- and 8-state codes

respectively. It should be noted that results for rms delay spread values greater than those indicated on the graphs are not included as they give no new information, and the performance is so bad in this range that it is deemed of no interest. These discarded results represent only eight of the total one hundred impulse responses.

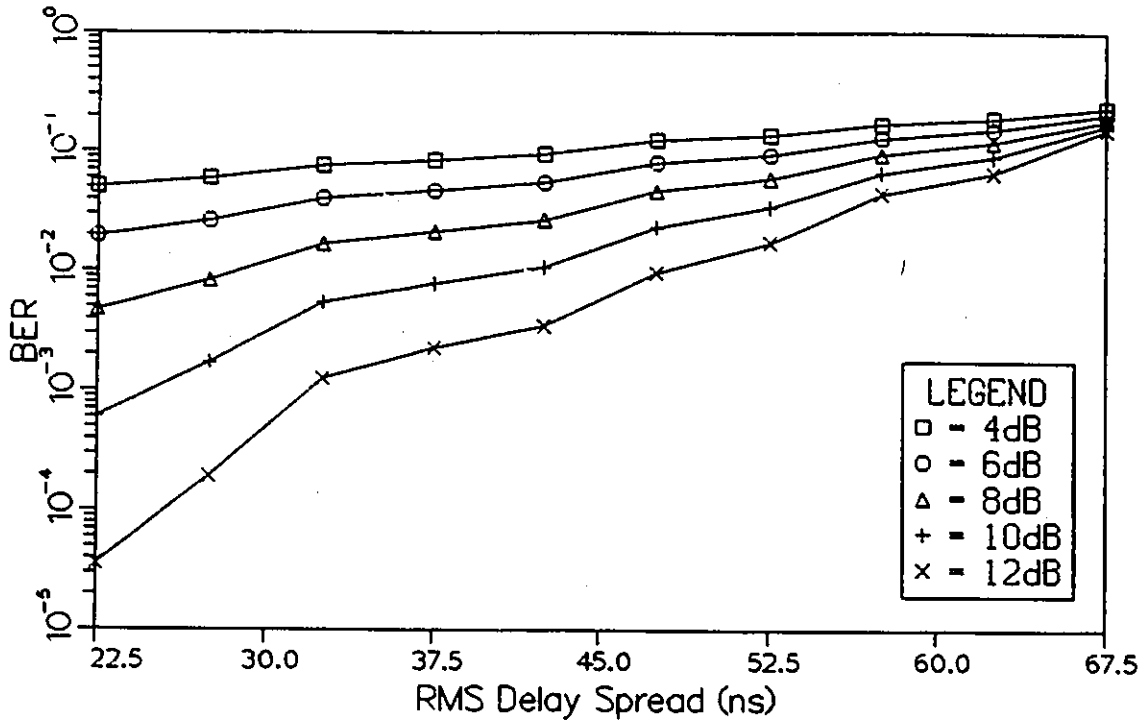

Figure 5.1: BER performance of DQPSK in the IW channel.

As can be expected, all three modulation schemes suffer from increasingly worse BER performance as the rms delay spread is increased. For small SNR values up to 8 dB, both 4- and 8-state TCM perform worse than DQPSK, as is seen in Figure 5.4, which is a different representation of the curves given in Figures 5.1, 5.2 and 5.3.

Beyond SNR = 8 dB, 8-state TCM performs better than the two other modulation schemes, but only for small values of rms delay spread. As shown in Figure 5.5, 4- and 8-state TCM perform better than DQPSK at a SNR of 10dB for $\sigma_T < 33$ ns ($\sigma_N < 0.165$). The performances improve in Figure 5.6 for 12dB, where TCM has a

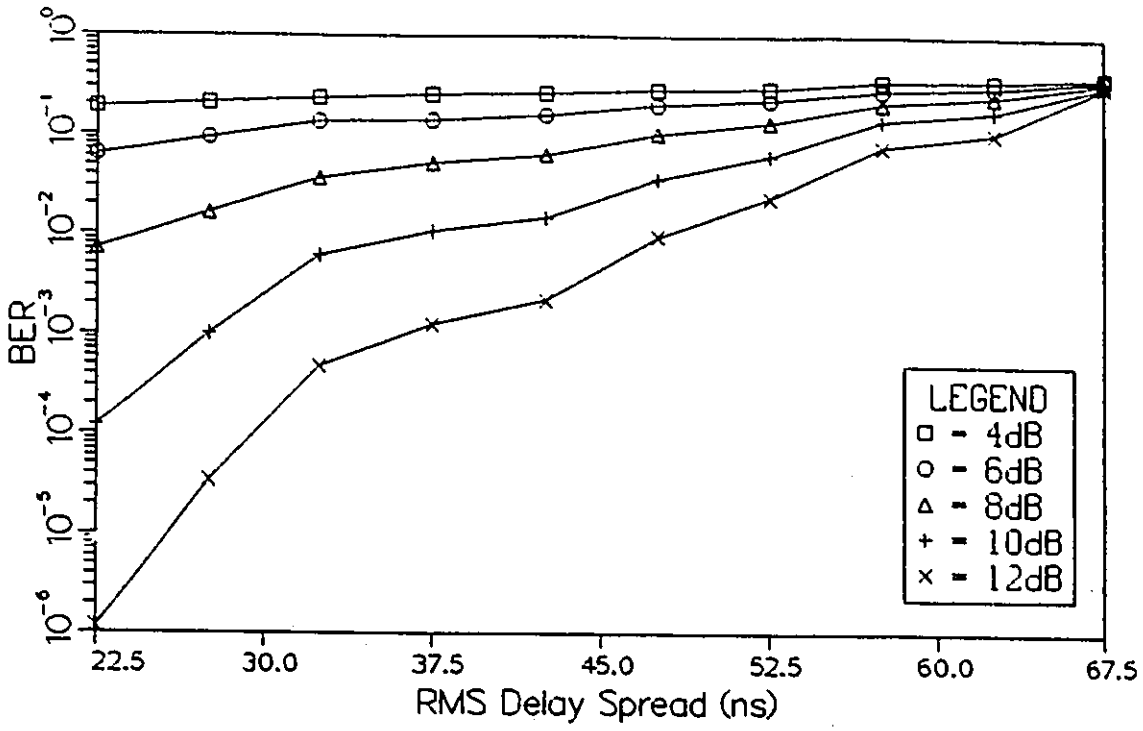

Figure 5.2: BER performance of 4-state TCM in the IW channel.

better BER performance than DQPSK for $\sigma_T < 49$ ns ($\sigma_N < 0.245$).

It is understandable that DQPSK is better than TCM for values of SNR up to 8 dB, since this is also the case for the Gaussian channel, as shown in Figure 3.8 of Section 3.3.3. This indicates that the 8 dB advantage limit which exists for the Gaussian channel has remained relatively unchanged by the dispersive channel.

Figure 5.6 also indicates that 8-state TCM achieves a BER of better than 10^{-4} for rms delay spreads σ_T of up to 31 ns ($\sigma_N \leq 0.155$) and SNR = 12 dB, whereas 4-state TCM achieves the same performance for $\sigma_T \leq 29$ ns and DQPSK for $\sigma_T \leq 25$ ns. The difference is not considerable but increases with higher SNR, as seen when comparing Figures 5.5 and 5.6. Simulations for SNR values beyond 12 dB were avoided because of the extensive computational time required.

A reliability criterion which is often used in the literature for the acceptable limit of

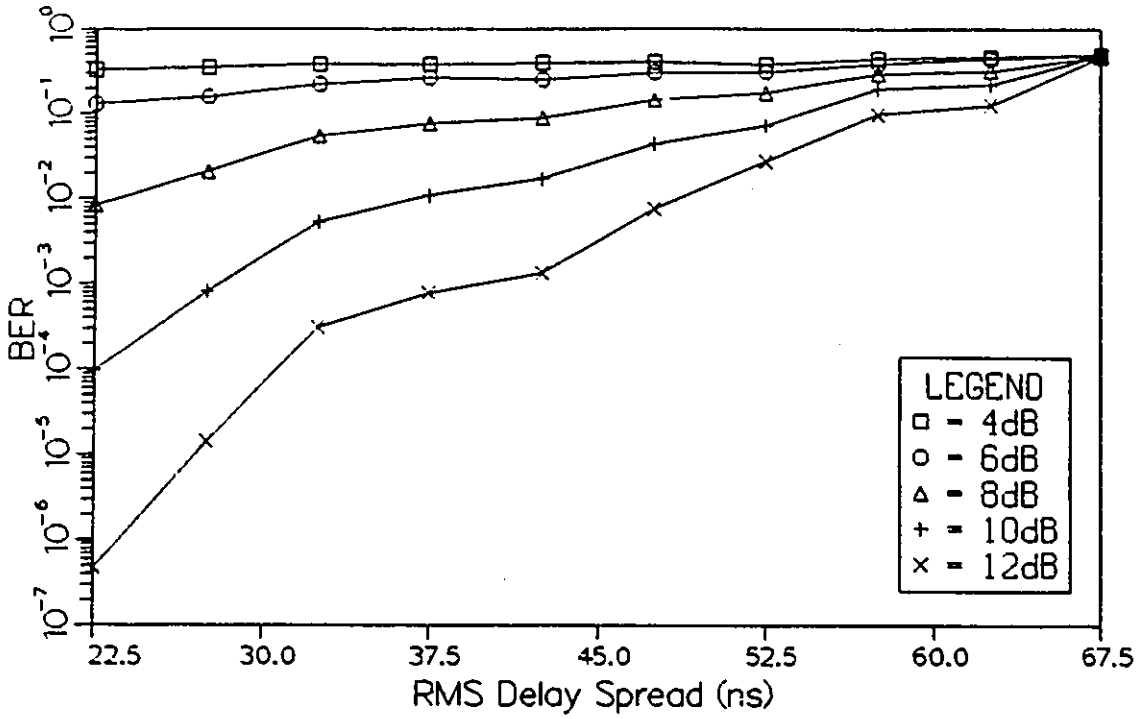

Figure 5.3: BER performance of 8-state TCM in the IW channel.

quality speech and data communications is a BER of 10^{-3}. This criterion is achieved at a 12 dB signal to noise ratio by the 8-state TCM for an rms delay spread value $\sigma_T \leq 41$ ns ($\sigma_N \leq 0.21$), by 4-state TCM for $\sigma_T \leq 37$ ns, and by DQPSK for $\sigma_T \leq 32$ ns.

When comparing the simulation results with the BER performance results by Chuang [9, 10], where the normalized rms delay spread σ_N is considered only up to 0.2, coherent QPSK is shown to have an irreducible BER of 6×10^{-3} for $\sigma_N = 0.2$ ($\sigma_T = 40$ ns). This is comparable with the BER of 3×10^{-3} obtained in our simulations for non-coherent QPSK at a SNR of 12 dB for $\sigma_N = 0.2$. Obviously, for increasing SNR, this BER will decrease a little until it reaches its irreducible value. Considering the penalty of using the non-coherent signaling in this study, one must assume that the more practical system configuration, such as using a carrier recovery loop for detection,

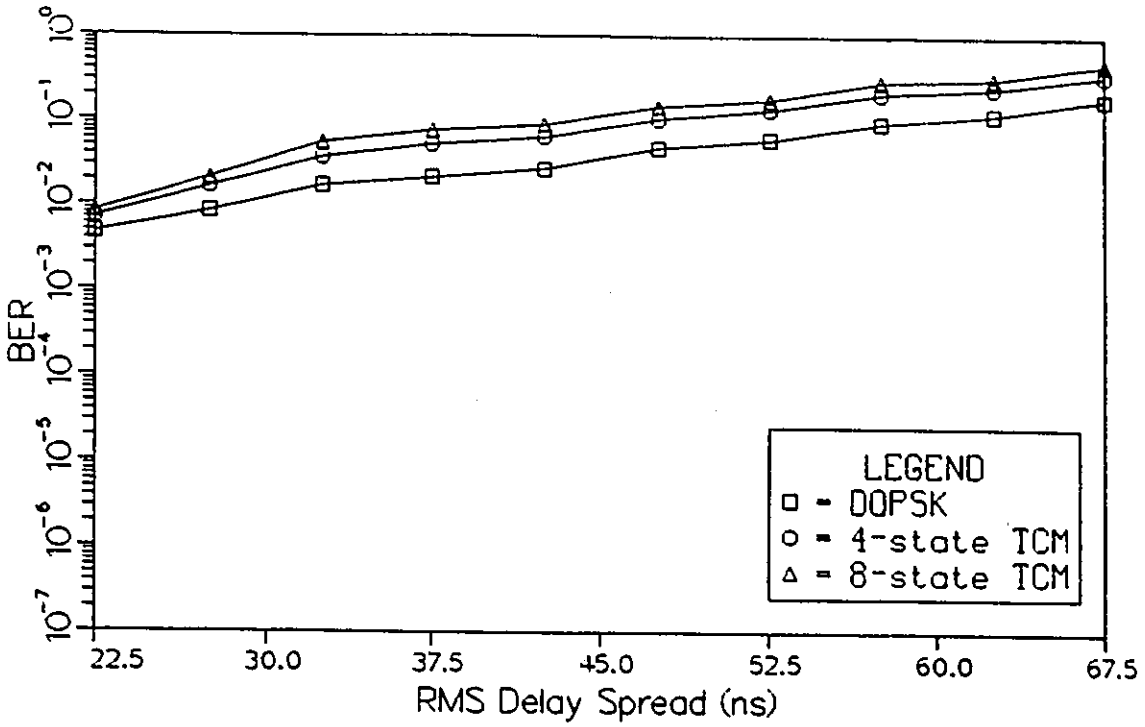

Figure 5.4: BER performance of 4- and 8-state TCM and DQPSK for SNR = 8 dB.

used in [9] manages to reduce the BER below the level obtained in our performance analysis.

Results given in [11] for coherent QPSK with a data rate R_b = 10 Mbits/s using a continuous channel model with an rms delay spread of σ_T = 35 ns (σ_N = 0.175) show a BER performance of about 3×10^{-3} at SNR = 20 dB, and 1×10^{-3} at 30 dB. These results are similar to the results in [9].

Another interpretation of the simulation results is presented in Figure 5.7, where the outage probability is given as a function of BER for DQPSK and 4- and 8-state 8-PSK TCM with SNR = 12 dB. The probability of outage is the fraction of time that the received signal will have a BER performance worse than a predetermined value. It also represents the distribution of the BER performance as obtained through simulations. Figure 5.7 indicates for instance that about 68% of cases suffer from outage at a BER

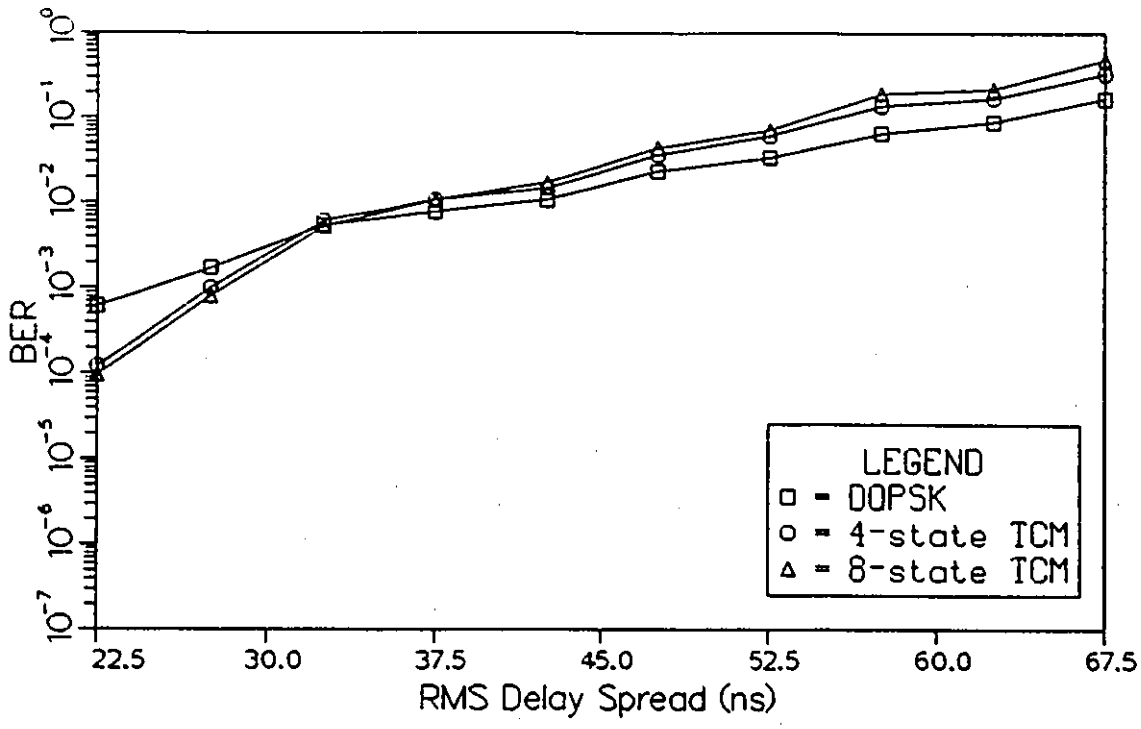

Figure 5.5: BER performance of 4- and 8-state TCM and DQPSK for SNR = 10 dB.

of 10^{-4} for both TCM codes, whereas for DQPSK, the outage probability is higher with 81% of the cases. All three schemes have an outage probability of about 62% for a BER of 10^{-3}.

This representation shows that TCM has lower outage probability, i.e. better performance, than DQPSK for BER$< 10^{-3}$, with the 8-state code giving lower outage probability than the 4-state code. When the BER is above 10^{-3}, DQPSK has a lower outage probability than both TCM codes, but this is a range of BER that is rather high for quality transmissions.

A similar representation of the outage probability measure is given in [9, 14], but direct comparisons are avoided due to the different system configurations. Results in [9] indicate that for raised cosine coherent QPSK with 25% rolloff and SNR = 30 dB, an outage probability of about 7% is achieved for BER$= 10^{-3}$, when $\sigma_T = 40$

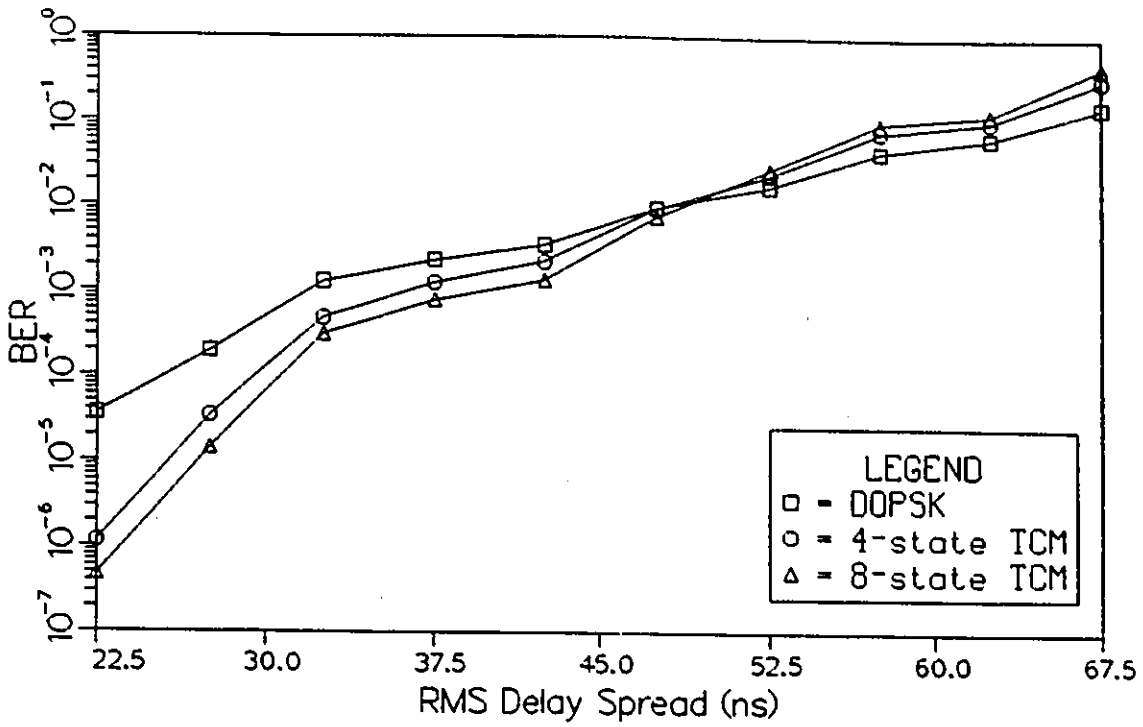

Figure 5.6: BER performance of 4- and 8-state TCM and DQPSK for SNR = 12 dB.

ns with R_b = 10 Mbits/s. The results given in Figure 5.7 represent the one hundred impulse responses, which have a mean rms delay spread of 46 ns. This study doesn't consider coherent signaling, or SNR values up to 30 dB, all of which give improved BER performance.

5.2 Performance with Linear Equalization

5.2.1 Fixed-Tap Equalizer

Since all relevant simulations for the fixed-tap equalizer are done with the approximated tap coefficient algorithm assuming that $N_0 = 0$ to simplify equalizer simulation set-up, it is first demonstrated that this is a legitimate practice for the SNR range considered, by showing that it has little effect on the performance results.

Simulations are performed on five different channel impulse response files (whose

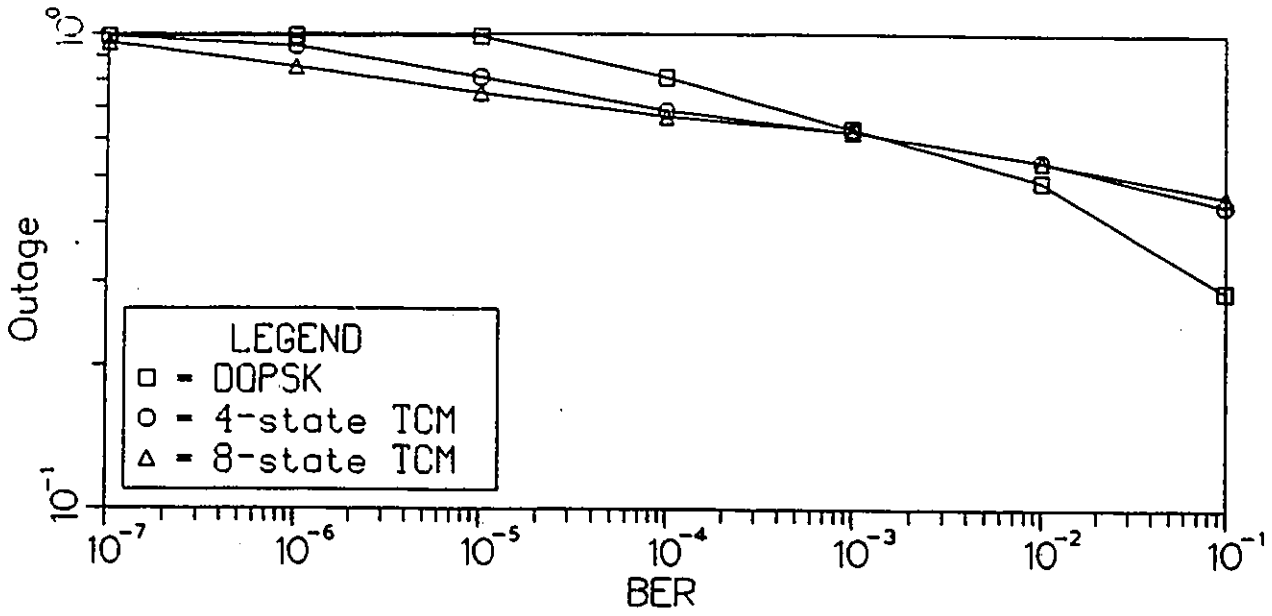

Figure 5.7: Outage probability versus BER for SNR = 12 dB.

rms delay spreads range from 35 to 52 ns) with 4-state TCM to evaluate the effect of the noise density parameter N_0 in the calculation of the equalizer tap weight coefficients. Using equation (2.16) with $N_0 = 0$ as an approximation, the tap weight coefficients are calculated and used in simulations for 3- and 5-tap configurations. BER performances are compared to the exact case without the $N_0 = 0$ approximation. The results as given in Figure 5.8 indicate that for the range of SNR considered, which is from 4 to 10dB, the BER performance is negligibly affected by the approximation of $N_0 = 0$ for both 3- and 5-taps. This is expected given the relation of N_0 and x_0 in equation (3.16). For this reason, subsequent simulations with the fixed-tap equalizer use the aforementioned approximation when calculating the tap-weight coefficients.

A series of simulations are executed with a fixed-tap equalizer to determine the impact of the number of taps on the BER performance for 4-state TCM. Seventeen

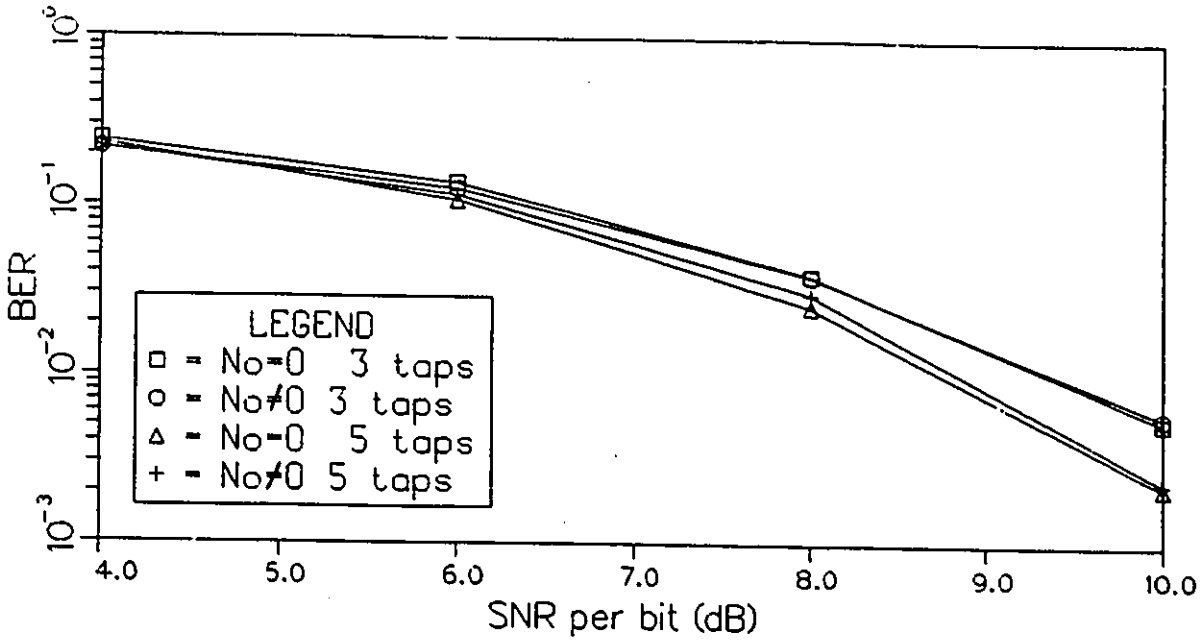

Figure 5.8: Effect of approximating the tap weight coefficients with $N_0 = 0$.

channel impulse responses characterized with very poor BER performance without the equalizer are used to give a representation of the equalizer's performance under worst case situations (Table A.1 in Appendix A indicates the files used), and the results are presented in Figure 5.9. As expected, a 5-tap equalizer gives a better performance than a 3-tap equalizer, but the relative improvement reduces as the number of taps increases; therefore the biggest improvement occurs when using only 3 taps. The performance achieved at SNR = 10 dB isn't very good: a BER of 5×10^{-3} for 5 taps, and 1.5×10^{-2} for 3 taps. It should be remembered that the impulse responses chosen for these simulations did not represent the average case, but rather the worst case, as indicated by the BER values for the system without equalization shown in Appendix A. They were chosen to show how the equalizer behaves in such situations, since these will be causing transmission problems and poorer performance than the average cases.

Further simulations are performed to see the effect of the fixed 3-tap equalizer for

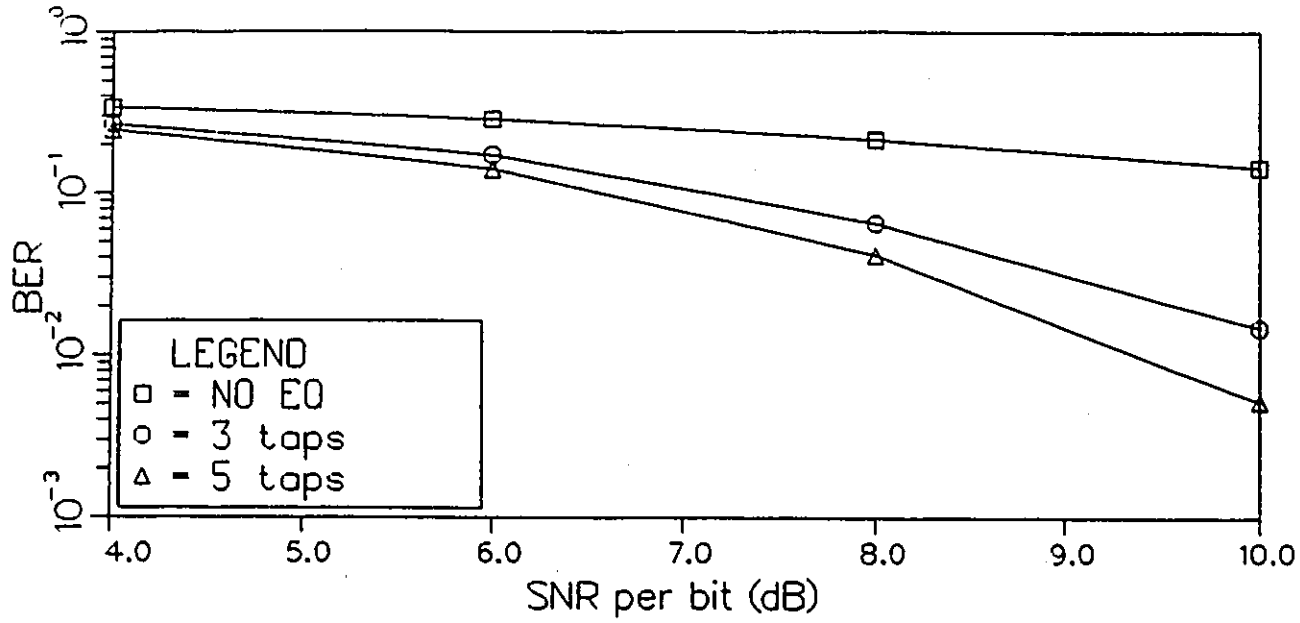

Figure 5.9: Effect of the number of taps on the BER performance.

DQPSK and differential TCM. Twenty-six representative channel impulse responses are chosen (see Table A.3 in Appendix A), and the results are presented in Figure 5.10, not as a function of rms delay spread, but as an overall performance, where all results are averaged together for specific SNR values. This is done because the twenty-six channel impulse responses were not sufficient to give a representative performance as a function of rms delay spread, and it was decided not to do simulations for all one hundred impulse responses because of time constraints.

The performance of 8-state TCM without the equalizer is seen in Figure 5.10 to be worse than both 4-state TCM and DQPSK without equalizer for the whole SNR range. This is so because the overall averaging includes channel impulse responses with rms delay spread values ranging from 26 to 80 ns, and it is shown in Figure 5.5 that for SNR = 10 dB, 8-state TCM outperforms the other schemes only for values of $\sigma_T < 33$ ns, so impulse responses with larger σ_T are influencing the averaging process.

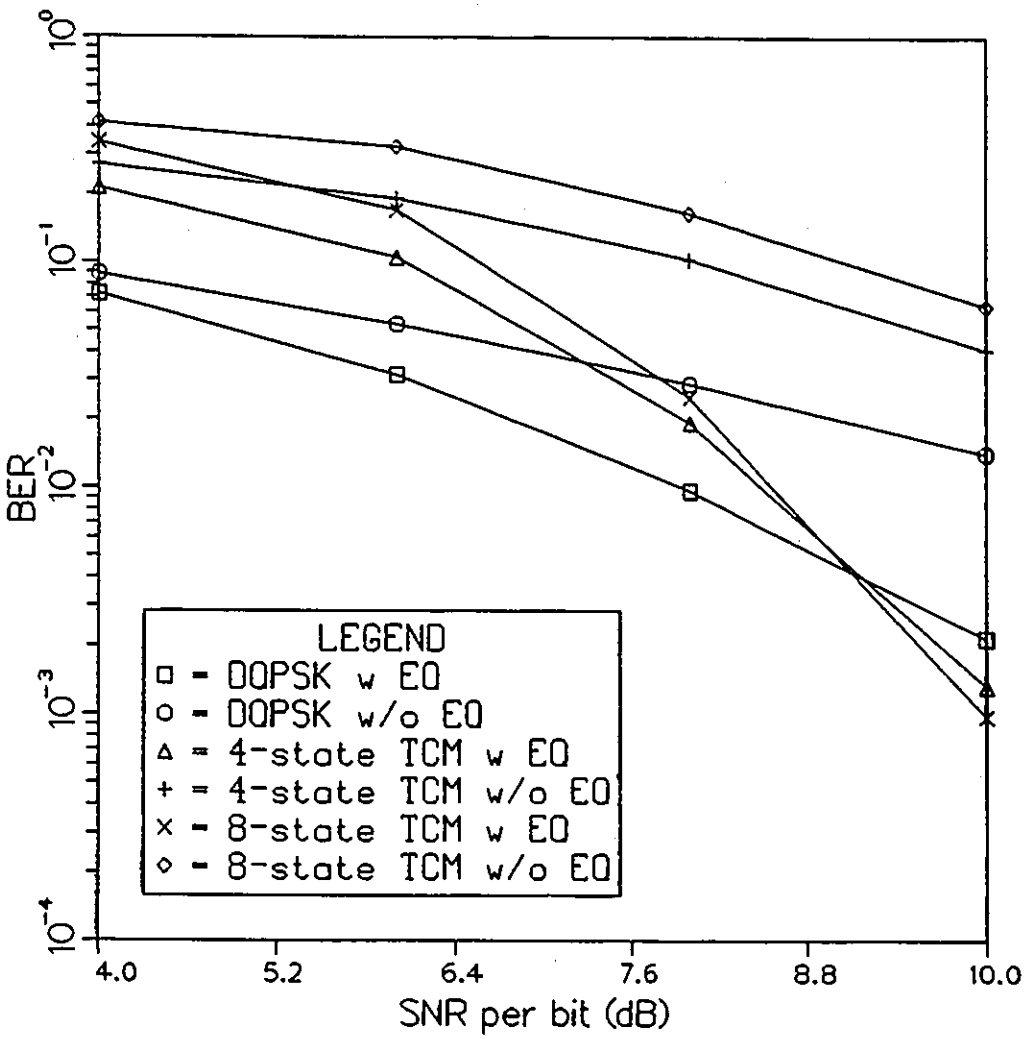

Figure 5.10: BER performance of DQPSK and TCM with the fixed-tap linear equalizer.

The performance with equalizer in Figure 5.10 increases sharply for 8-state TCM, more so than for the other schemes. It is found that with SNR = 10 dB, the use of a fixed-tap equalizer increases the performance with a reduction in BER of about six-fold for DQPSK, a factor of 28 for 4-state TCM and sixty times for 8-state TCM. The curves for DQPSK and 4- and 8-state TCM with the equalizer take on the same general form as the curves without equalizer for the Gaussian channel presented in Figure 3.8, but with the "8-PSK TCM/DQPSK advantage point" moved to around SNR = 9 dB, from 8 dB for the Gaussian channel. This is the SNR point above which 8-PSK TCM is advantageous to use relative to DQPSK. This shows that the fixed-tap equalizer considerably reduces the ISI impairment due to the fading multipath indoor wireless channel.

5.2.2 Adaptive Equalizer

Since fixed-tap linear equalizers cannot be used in practice on a time-varying channel, the adaptive linear filter is now considered. It is used in a 3-tap configuration with DQPSK for six channel impulse responses (see Table A.2 in Appendix A) to compare its performance with a fixed-tap linear equalizer.

Figure 5.11 presents results averaged over these six impulse responses for the adaptive 3-tap equalizer, the fixed 3-tap equalizer, and no equalizer. It can be seen that the adaptive equalizer outperforms the fixed equalizer only for BER values below 5×10^{-3}. Therefore, the adaptive equalizer should be used with low BER (i.e. SNR $\geq$ 8.3 dB) to achieve a performance advantage. Note that BER values higher than 5×10^{-3} represent unacceptable performance for data communication systems, so for the BER range of interest, the adaptive equalizer will always outperform the fixed-tap equalizer.

Figure 5.11 also indicates that a significant advantage can be obtained at higher

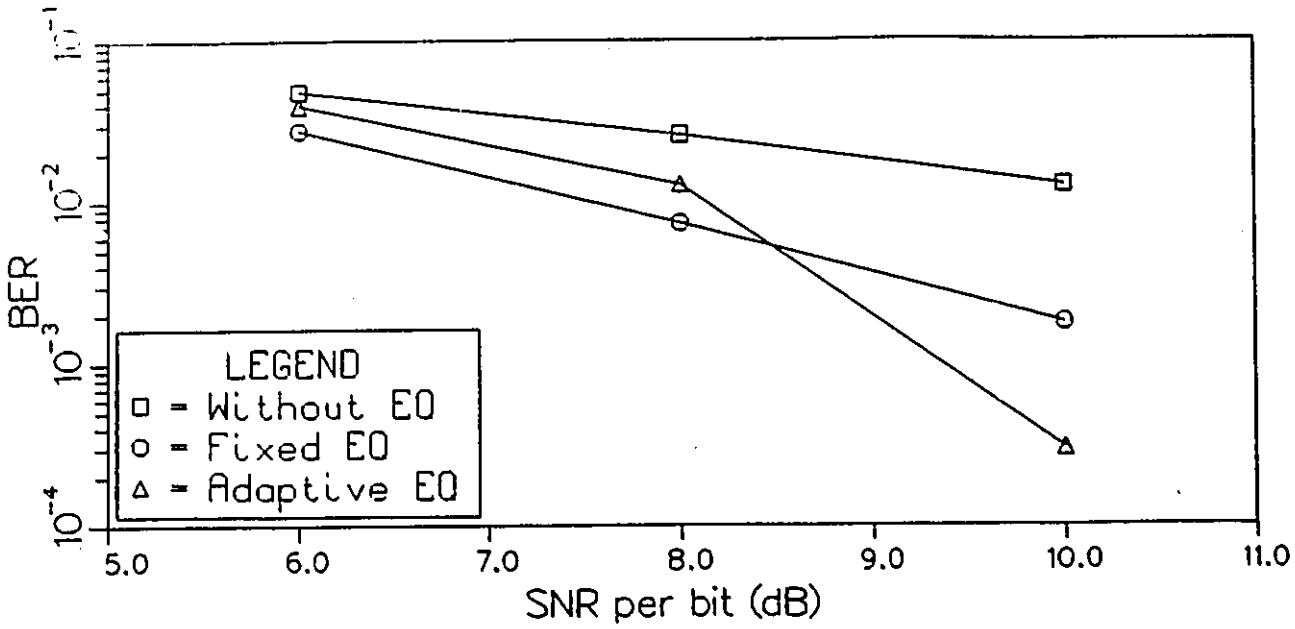

Figure 5.11: BER performance of DQPSK with the adaptive equalizer.

SNR by using the adaptive equalizer instead of the fixed-tap equalizer, whose tap weight coefficients are calculated theoretically from the known channel parameters. Considering that this study used fixed channel impulse responses, this may be partly explained by the fact that the adaptive process compensates with knowledge of the decision device output and the error measure, whereas the fixed equalizer blindly compensates independently of the received data.

As mentioned earlier, adaptive equalization applied to a trellis coded modulation system is not considered because of complexity issues. The TCM introduces a decoding delay, in this case of either 12 or 18 symbols for the 4- and 8-state cases respectively, and this must be dealt with by various schemes, otherwise the adaptive process will wrongly correct the input for the interference that occured 12 or 18 symbols ago, thereby increasing the errors.

5.3 Summary

The BER performance results obtained through simulation are presented. It is shown that for SNR values beyond 8 dB and low rms delay spreads, differential TCM outperforms DQPSK. As the rms delay spread increases, the performance advantage of TCM diminishes, until it completely disappears and DQPSK eventually has the advantage. This crossover point depends on the SNR.

The linear equalizer considerably improves the BER performance by reducing the effect of intersymbol interference on the information signal. Increasing the number of taps increases this performance, however any additional improvement decreases as the number of taps increases. 8-state TCM with the fixed-tap linear equalizer is seen to perform better than DQPSK at higher SNR, even when the channel suffers from considerable rms delay spread.

It is concluded that the adaptive equalizer's advantage over the fixed-tap equalizer occurs for all cases where the BER is in the range of interest, usually below 10^{-3}. This makes it the equalizer of choice for any DQPSK design, as it outperforms the fixed configuration over the BER range of interest. The implementation of adaptive equalization in a TCM system was avoided in this work because of the previously discussed complexity issues involved.

Chapter 6

Conclusions

6.1 Summary

The indoor wireless channel is known to suffer from fading and dispersion due to movement and multipath propagation. This dispersion presents itself as intersymbol interference, which limits the maximum data rate and causes irreducible BER performance.

A statistical model is presented to describe and represent the behaviour of an indoor wireless communications channel. The line-of-sight components are not considered in this model, and a Rayleigh distribution is chosen to represent the path gains. The rms delay spread measure of the impulse response is seen to characterize the dispersiveness of this channel model.

Methods of reducing the channel's impairments are considered: interleaving is seen to be unsuited to the slow-fading IW environment; antenna or polarization diversity, though not used in this study because the channel is considered quasi-stationary, should normally be considered as important schemes to reduce the effect of fading in a practical system. Channel coding is used in the form of trellis-coded modulation, a useful technique to achieve performance gains in a bandwidth-constrained IW channel. Equalization is also considered in its linear transversal configuration to reduce the

effect of ISI caused by the multipath channel.

The codes used for error control are differential 4- and 8-state PSK TCM and their performance is compared with that of DQPSK modulation. A decoding depth of $D = 6\nu$ is used for all simulations unless otherwise stated.

Differential signaling is not optimal due to the multiplication of two consecutive waveforms, which has the following effects: the noise at the output is non-Gaussian, the system suffers from an effective rms delay spread that is larger than the actual value, and the Euclidean distance becomes a sub-optimum metric for the Viterbi decoder. Even with all these problems, differential signaling is still used to avoid the requirements of the channel phase distortion information and because coherent detection can be difficult to achieve in practice during fades.

It is also mentioned that the Euclidean distance is not optimal for use with fading channels, but it is used because of its simplicity. Furthermore the 8-state 8-PSK TCM code used in the simulations, designed for the Gaussian channel using the Euclidean distance, is also optimal for fading channels.

Linear equalization is applied to the TCM and DQPSK systems. Both fixed-tap and adaptive transversal equalizers are considered. Most BER performance improvement occurs with the 3-tap configuration, though the performance still increases for higher tap numbers. Adaptive equalization is seen to be advantageous for low BER values. Attention must be given to the step-size parameter of the iterative process, to ensure proper convergence.

Beyond the problems already mentioned related to the use of differential detection, another problem occurs with the use of a DFE due to the non-linearity of the detector in the feedback loop. To consider a DFE as described in the literature, coherent signaling must be used. Though the DFE is not considered in the simulation study, it is known

to outperform the transversal equalizer for the practical case of the time-varying IW channel, which suffers from spectral nulls.

6.2 Concluding Remarks

The differential 4- and 8-state 8-PSK TCM are found to outperform DQPSK for SNR values above 8 dB and low rms delay spreads. This performance advantage exists for higher rms delay spreads when the SNR is increased. TCM also suffers from less outage than DQPSK for BER values below 10^{-3}.

For applications where BER values in the range of 10^{-3} are acceptable, such as voice transmission, TCM would have very little if any advantage. However, for cases such as data communications, where a BER value in the range of 10^{-5} is required, there is an obvious advantage with TCM.

These results can be extrapolated to coherent detection. It is known that differential detection imposes a reduction on the BER performance. Knowing that the Euclidean metric is the optimal decoding criteria for coherent detection but not for differential detection, it is expected that the BER performance advantage of TCM with coherent detection will be greater than that found with differential detection.

Spread spectrum, as studied in the literature, offers very interesting ISI mitigating capabilities that makes it perform better than most other non-spreading modulation schemes, but it requires a large bandwidth. For bandwidth-constrained situations, TCM might be a better choice, though this selection depends on many other factors, such as receiver complexity and power constraints.

Equalization is seen to considerably reduce the effect of ISI caused by the multipath channel. A fixed 3-tap linear equalizer is shown to give performance curves reminiscent of the curves for the Gaussian channel, where TCM has better BER performance than

DQPSK for SNR values above 8dB.

The adaptive transversal equalizer is found to outperform the fixed-tap linear equalizer for BER values below 10^{-3}. It is known from literature that adaptive DFE is better than the adaptive linear equalizer when used in the indoor wireless channel.

Thus, TCM with equalization can achieve considerable BER performance in the presence of channel dispersion, measured as rms delay spread.

6.3 Recommendations for Future Research

Many other facets of this subject would make for interesting research.

The use of coherent signaling could be considered for comparison with the present results for differential signaling.

Though diversity isn't used because the channels are considered quasi-stationary, it should be implemented for a time-varying channel that suffers from slow-fading, such as the indoor wireless channel.

The use of an adaptive DFE with TCM and a measure of its performance relative to the transversal equalizer would be interesting, and might possibly be implemented using a software application such as the one presented in reference [35] (developed specifically for such indoor wireless applications).

One further item of interest for simulation is the development of a dynamic IW channel model to permit more realistic simulations. Such a model could possibly be obtained through the autoregressive frequency domain statistical model mentioned briefly in section (2.2). This model is developed to have very few parameters, namely two, so a dynamic version could be feasible with this model, unlike with the time-domain model used, which can have up to a few hundred complex impulse response components. This would make a dynamic model more feasible.

Appendix A

Tables of Impulse Response Files used for Equalization Simulations

This appendix contains the channel impulse responses used in simulations to obtain the BER performance of the systems with equalization.

Table A.1 presents seventeen channel impulse responses characterized by very poor BER performance. They are used for simulations in Section 5.2 to determine the dependence of the number of equalizer taps on the BER performance with 4-state TCM; they are selected to show that equalization does have an advantage even in very bad environments. The BER performance given in this table at SNR = 10 dB is for the 4-state TCM system without equalizer. Results of the simulations for various SNR with 3 and 5 tap equalizers are given in Figure 5.9.

Table A.2 presents six typical channel impulse responses used for simulations in Section 5.2, to determine the BER performance of the adaptive linear equalizer with 4-state TCM. Results of the simulations for various SNR with the adaptive equalizer are given in Figure 5.11.

Table A.3 presents twenty-six representative channel impulse responses used for simulations in Section 5.2, to determine the BER performance of the fixed 3-tap linear equalizer with 4- and 8-state TCM and DQPSK. The BER results given in this table are

File	σ_1 (ns)	BER at SNR = 10dB
60	33.05	2.55×10^{-1}
55	35.61	2.14×10^{-2}
93	36.09	2.13×10^{-1}
30	40.64	8.99×10^{-2}
8	40.76	3.59×10^{-1}
48	45.49	4.37×10^{-1}
6	48.10	4.79×10^{-1}
31	49.18	4.76×10^{-1}
24	50.70	3.68×10^{-2}
19	51.34	2.31×10^{-1}
16	51.73	4.12×10^{-1}
17	51.84	1.21×10^{-1}
21	54.11	2.33×10^{-2}
15	55.08	4.98×10^{-1}
22	61.07	4.45×10^{-1}
10	61.63	4.41×10^{-3}
86	79.60	1.82×10^{-1}

Table A.1: Channel impulse responses characterized by very poor 4-state TCM BER performance used in simulations to determine the dependence of the number of taps on the BER performance.

for these three schemes at SNR = 10 dB without equalizer. Results of the simulations for various SNR with equalization are given in Figure 5.10.

File	σ_T (ns)
59	25.65
55	35.61
30	40.64
51	45.62
24	50.70
80	57.38

Table A.2: Channel impulse responses used in simulations to determine the BER performance of the adaptive linear equalizer.

File	σ_T (ns)	4-state TCM	8-state TCM	DQPSK
59	25.65	2.69×10^{-2}	4.54×10^{-2}	1.11×10^{-2}
97	27.32	2.62×10^{-2}	4.36×10^{-2}	1.07×10^{-2}
64	28.92	1.92×10^{-1}	3.28×10^{-1}	4.21×10^{-2}
60	33.05	2.55×10^{-1}	3.76×10^{-1}	7.33×10^{-2}
55	35.61	2.14×10^{-2}	2.52×10^{-2}	9.96×10^{-3}
93	36.09	2.13×10^{-1}	2.46×10^{-1}	4.50×10^{-2}
25	37.61	7.81×10^{-2}	1.47×10^{-1}	2.03×10^{-2}
90	38.92	4.57×10^{-3}	3.78×10^{-3}	3.74×10^{-3}
30	40.64	8.99×10^{-2}	1.64×10^{-1}	2.26×10^{-2}
96	43.78	3.29×10^{-2}	6.93×10^{-2}	1.19×10^{-2}
92	44.18	6.17×10^{-2}	1.04×10^{-1}	1.58×10^{-2}
51	45.62	1.81×10^{-2}	5.02×10^{-2}	8.13×10^{-3}
49	46.48	8.77×10^{-3}	8.27×10^{-3}	4.48×10^{-3}
56	46.58	8.52×10^{-2}	9.58×10^{-2}	2.07×10^{-2}
45	46.68	9.06×10^{-3}	2.07×10^{-2}	5.89×10^{-3}
24	50.70	3.68×10^{-2}	6.72×10^{-2}	1.13×10^{-2}
19	51.34	2.31×10^{-1}	3.84×10^{-1}	5.67×10^{-2}
17	51.84	1.21×10^{-1}	1.66×10^{-1}	2.71×10^{-2}
21	54.11	2.33×10^{-2}	4.70×10^{-2}	8.66×10^{-3}
41	56.46	4.14×10^{-3}	4.09×10^{-3}	2.85×10^{-3}
40	56.78	1.64×10^{-1}	3.37×10^{-1}	3.56×10^{-2}
80	57.38	5.97×10^{-2}	1.23×10^{-1}	1.70×10^{-2}
10	61.63	4.41×10^{-3}	5.66×10^{-3}	3.26×10^{-3}
77	70.61	1.28×10^{-1}	2.04×10^{-1}	2.63×10^{-2}
83	73.83	9.26×10^{-3}	1.08×10^{-2}	6.17×10^{-3}
86	79.62	1.82×10^{-1}	3.44×10^{-1}	3.60×10^{-2}

Table A.3: Channel impulse responses used in simulations to determine the BER performance of the fixed 3-tap linear equalizer.

Bibliography

[1] Cox D.C., "Universal Digital Portable Radio Communications," *Proc. IEEE*, vol.75, no.4, pp.436-477, April 1987.

[2] Cox D.C., Arnold H.W., Porter P.T., "Universal Digital Portable Communications: A System Perspective," *IEEE J. Selec. Areas Commun.*, vol.5, no.5, pp.764-773, June 1987.

[3] Cox D.C., "Personal Communications - A Viewpoint," *IEEE Commun. Mag.*, vol.28, no.11, p.8, Nov. 1990.

[4] Acampora A.S., Winters J.H., "A Wireless Network for Wide-band Indoor Communications," *IEEE J. Selec. Areas Commun.*, vol.5, no.5, pp.796-805, June 1987.

[5] Acampora A.S., Winters J.H., "System Applications for Wireless Indoor Communications," *IEEE Commun. Mag.*, vol.25, no.8, pp.11-20, Aug. 1987.

[6] Howard S.J., Pahlavan K., "Performance of a DFE Modem Evaluated from Measured Indoor Radio Multipath Profiles," *Proc. IEEE ICC '90*, pp.1341-1345, 1990.

[7] Despins C.L., Falconer D.D., Mahmoud S.A., "Coding and Optimum Baseband Combining for Wideband TDMA Indoor Wireless Channels," *Proc. IEEE Globecom 1990*, pp.902.7.1-902.7.6, 1990.

[8] Chuang J.C.-I., "Simulation of Digital Modulation on Portable Radio Communications Channels with Frequency-Selective Fading," *Proc. IEEE Globecom '86*, pp.1120-1126, 1986.

[9] Chuang J.C.-I., "The Effects of Time Delay Spread on Portable Radio Communications Channels with Digital Modulation," *IEEE J. Selec. Areas Commun.*, vol.5, no.5, pp.879-889, June 1987.

[10] Chuang J.C.-I., "Comparison of Coherent and Differential Detection of BPSK and QPSK in a Quasistatic Fading Channel," *IEEE Trans. Commun.*, vol.38, no.5, pp.565-567, May 1990.

[11] Sexton T.A., Pahlavan K., "Channel Modelling and Adaptive Equalization of Indoor Radio Channels," *IEEE J. Selec. Areas Commun.*, vol.7, no.1, pp.114-121, Jan. 1989.

[12] Saleh A.A.M., Cimini L.J.Jr, "Indoor Radio Communications using Time-Division Multiple Access with Cyclical Slow Frequency Hopping and Coding," *IEEE J. Selec. Areas Commun.*, vol.7, no.1, pp.59-70, Jan. 1989.

[13] Saleh A.A.M., Rustako A.J.Jr, Cimini L.J.Jr. Owens G.J., Roman R.S., "An Experimental TDMA Indoor Radio Communications System Using Slow Frequency Hopping and Coding," *IEEE Trans. Commun.*, vol.39, no.1, pp.152-162, Jan. 1991.

[14] Valenzuela R.A., "Performance of Quadrature Amplitude Modulation for Indoor Radio Communications," *IEEE Trans. Commun.*, vol.35, no.11, pp.1236-1238, Nov. 1987.

[15] Valenzuela R.A., "Performance of Adaptive Equalization for Indoor Radio Communications," *IEEE Trans. Commun.*, vol.37, no.3, pp.291-293, March 1989.

[16] Kavehrad M., Ramamurthi B., "Direct-Sequence Spread Spectrum with DPSK Modulation and Diversity for Indoor Wireless Communications," *IEEE Trans. Commun.*, vol.35, no.2, pp.224-236, Feb. 1987.

[17] Kavehrad K., McLane P.J., "Spread Spectrum for Indoor Digital Radio," *IEEE Commun. Mag.*, vol.25, no.6, pp.32-40, June 1987.

[18] Kavehrad M., Bodeep G.E., "Design and Experimental Results for a Direct-Sequence Spread-Spectrum Radio Using Differential Phase-Shift Keying Modulation for Indoor, Wireless Communications," *IEEE J. Selec. Areas Commun.*, vol.5, no.5, pp.815-823, June 1987.

[19] Du J., Vucetic B., Zhang L., "New 16PSK Trellis Codes for Fading Channels," *Proc. Int. Mobile Satellite Conf.*, pp.481-486, Ottawa, 1990.

[20] Lee A.C., McLane P.J., "Convolutionally Interleaved PSK and DPSK Trellis Codes for Shadowed, Fast Fading Mobile Satellite Communication Channels," *IEEE Trans. Veh. Technol.*, vol.39, no.1, pp.37-47, Feb. 1990.

[21] McLane P., Wittke P.H., Ho P.K.-M., Loo C., "PSK and DPSK Trellis Codes for Fast Fading, Shadowed Mobile Satellite Communication Channels," *Proc. IEEE ICC '87*, pp.726-731, 1987.

[22] McLane P., Wittke P.H., Ho P.K.-M., Loo C., "PSK and DPSK Trellis Codes for Fast Fading, Shadowed Mobile Satellite Communication Channels," *IEEE Trans. Commun.*, vol.36, no.11, pp.1242-1246, Nov. 1988.

[23] Wilson S.G., Leung Y.S., "Trellis-Coded Phase Modulation on Rayleigh Channels," *Proc. IEEE ICC '87*, pp.739-743, 1987.

[24] Saleh A.A.M., Valenzuela R.A., "A Statistical Model for Indoor Multipath Propagation," *IEEE J. Selec. Areas Commun.*, vol.5, no.2, pp.128-137, Feb. 1987.

[25] Cox D.C., "Antenna Diversity Performance in Mitigating the Effects of Portable Radiotelephone Orientation and Multipath Propagation," *IEEE Trans. Commun.*, vol.31, no.5, pp.620-628, May 1983.

[26] Proakis J., *Digital Communications.*, McGraw-Hill, 1989.

[27] Turin G.L., Clapp F.D., Johnston T.L., Fine S.B., Lavry D., "A Statistical Model of Urban Multipath Propagations," *IEEE Trans. Veh. Technol.*, vol.21, pp.1-9, Feb. 1972.

[28] Bultitude R.J.C., "Measurement, Characterization and Modelling of Indoor 800/900 MHz Radio Channels for Digital Communications," *IEEE Commun. Mag.*, vol.25, no.6, pp.5-12, June 1987.

[29] Lee W.C.Y., *Mobile Communications Engineering*, McGraw-Hill, 1982.

[30] Alexander S.E., "Radio Propagation Within Buildings at 900 MHz," *Electron. Lett.*, vol.18, no.21, pp.913-914, 14 Oct. 1982.

[31] Alexander S.E., "Radio Propagation Within Buildings at 900 MHz," *Proc. 3rd Int. Conf. Antennas Propagat.*, pp.177-180, 1983.

[32] Alexander S.E., "Characterizing Buildings for Propagation at 900 MHz," *Electron. Lett.*, vol.19, no.20, p.860, 29 Sept. 1983.

[33] Ganesh R., Pahlavan K., "On the Modeling of Fading Multipath Indoor Radio Channels," *Proc. IEEE Globecom '89*, pp.1346-1350, 1989.

[34] Howard S.J., Pahlavan K., "Statistical Autoregressive Models for the Indoor Radio Channel," *Proc. IEEE Globecom '90*, pp.1000-1006, 1990.

[35] Seidel S.Y., Rappaport T.S., *SIRCIM: A Novel Radio Channel Simulator for Indoor Microcellular Communication System Design*, Mobile & Portable Radio Research Group Report MPRG-TR-90-6, 1990.

[36] Winters J.H., Yeh Y.S., "On the Performance of Wideband Digital Radio Transmission Within Buildings using Diversity," *Proc. IEEE Globecom 1985*, vol.2, pp.991-996, 1985.

[37] Cox D.C., "Delay Doppler Characteristics of Multipath Propagation at 910 MHz in a Suburban Mobile Radio Environment," *IEEE Trans. Antennas Propagat.*, vol.20, no.5, pp.625-635, Sept. 1972.

[38] Devasirvatham D.M.J., "Time Delay Spread Measurements of Wideband Radio Signals Within a Building," *Electron. Lett.*, vol.20, no.23, pp.950-951, 8 Nov. 1984.

[39] Devasirvatham D.M.J., "Time Delay Spread Measurements of 850 MHz Radio Waves in Building Environments," *Proc. Globecom 1985*, pp.970-973, 1985.

[40] Devasirvatham D.M.J., "Time Delay Spread and Signal Level Measurements of 850 MHz Radio Waves in Building Environments," *IEEE Trans. Antennas Propagat.*, vol.34, no.11, pp.1300-1305, Nov. 1986.

[41] Devasirvatham D.M.J., "A Comparison of Time Delay Spread Measurements Within Two Dissimilar Office Buildings," *Proc. ICC 1986*, pp.852-857, 1986.

[42] Devasirvatham D.M.J, "A Comparison of Time Delay Spread and Signal Level Measurements Within Two Dissimilar Office Buildings," *IEEE Trans. Antennas Propagat.*, vol.35, no.3, pp.319-324, March 1987.

[43] Rappaport T.S., "Indoor Radio Communications for Factories of the Future," *IEEE Commun. Mag.*, vol.27, no.5, pp.15-24, May 1989.

[44] Rappaport T.S., "Characterization of UHF Multipath Radio Channels in Factory Buildings," *IEEE Trans. Antennas Propagat.*, vol.37, no.8, pp.1058-1069, Aug. 1989.

[45] Bultitude R., Mahmoud S.A., Sullivan W.A., "A Comparison of Indoor Radio Propagation Characteristics at 910 MHz and 1.75 GHz," *IEEE J. Selec. Areas Commun.*, vol.7, no.1, Jan. 1989.

[46] Jakes W.C. *Microwave Mobile Communications*, Wiley-Interscience Publications, 1974.

[47] Motley A.J., Alexander S.E., "Diversity Advantage for Cordless Telephones," *Electron. Lett.*, vol.19, no.14, pp.531-533, 7 July 1983.

[48] "Ethereal Networking: look, Ma, no wires," *IEEE Spectrum*, vol.26, no.4, pp.12, April 1989.

[49] Bergmann S.A., Arnold H.W., "Polarization Diversity in Portable Communications Environment," *Electron. Lett.*, vol.22, no.11, pp.609-610, 22 May 1986.

[50] Lin S., Costello, D.J.Jr., *Error Control Coding: Fundamentals and Applications*, Prentice-Hall, New Jersey, 1983.

[51] Ungerboeck G., "Trellis-Coded Modulation with Redundant Signal Sets, Part I: Introduction," *IEEE Commun. Mag.*, vol.25, no.2, pp.5-11, Feb. 1987.

[52] Forney G.D.Jr, Gallager R.G., Lang G.R., Longstaff F.M., Qureshi S.U., "Efficient Modulation for Band-Limited Channels," *IEEE J. Selec. Areas Commun.*, vol.2, no.5, pp.632-647, Sept. 1984.

[53] Pahlavan K., "Wireless Communications for Office Information Networks," *IEEE Commun. Mag.*, vol.23, no.6, pp.19-27, June 1985.

[54] Saleh A.A.M., Rustako A.J.Jr, Roman R.S., "Distributed Antennas for Indoor Radio Communications," *IEEE Trans. Commun.*, vol.35, no.12, pp.1245-1251, Dec. 1987.

[55] Feher K., *Digital Communications: Satellite/Earth Station Engineering*, Prentice-Hall, 1983.

[56] Ungerboeck G., "Channel Coding with Multilevel/Phase Signals," *IEEE Trans. Inform. Theory*, vol.28, no.1, pp.56-67, Jan. 1982.

[57] Ungerboeck G., "Trellis-Coded Modulation with Redundant Signal Sets, Part II: State of the Art," *IEEE Commun. Mag.*, vol.25, no.2, pp.12-21, Feb. 1987.

[58] Schwartz M., *Information Transmission, Modulation, And Noise*, McGraw-Hill, NY, 1990.

[59] Benedetto S., Marsan M.A., Albertengo G., Giachin E., "Combined Coding and Modulation: Theory and Applications," *IEEE Trans. Inform. Theory*, vol.34, no.2, pp.223-236, March 1988.

[60] Forney G.D., "The Viterbi Algorithm," *Proc. IEEE*, vol.61, no.3, pp.268-278, March 1973.

[61] Hayes J.F., "The Viterbi Algorithm Applied to Digital Data Transmission," *IEEE Commun. Mag.*, vol.13, no.3, pp.15-20, March 1975.

[62] Forney G.D.Jr, "Convolutional Codes II. Maximum-Likelihood Decoding," *Inform. Control*, vol.25, pp.222-266, July 1974.

[63] Fettweis G., Meyr H., "A 100 Mbit/s Viterbi Decoder Chip: Novel Architecture and its Realization," *Proc. IEEE ICC '90*, pp.463-467, 1990.

[64] Zehavi E., Wolf J.K., "On the Performance Evaluation of Trellis Codes," *IEEE Trans. Inform. Theory*, vol.33, no.2, pp.196-202, March 1987.

[65] Edbauer F., "Performance of Interleaved Trellis-Coded Differential 8-PSK Modulation over Fading Channels," *IEEE J. Selec. Areas Commun.*, vol.7, no.9, pp.1340-1346, Dec. 1989.

[66] Divsalar D., Simon M.K., "The Design of Trellis Coded MPSK for Fading Channels: Performance Criteria," *IEEE Trans. Commun.*, vol.36, no.9, pp.1004-1012, Sept. 1988.

[67] Divsalar D., Simon M.K., "The Design of Trellis Coded MPSK for Fading Channels: Set Partitioning for Optimum Code Design," *IEEE Trans. Commun.*, vol.36, no.9, pp.1013-1021, Sept. 1988.

[68] Schlegel C., Costello D.J.Jr, "Bandwidth Efficient Coding for Fading Channels: Code Construction and Performance Analysis," *IEEE J. Selec. Areas Commun.*, vol.7, no 9, pp.1356-1368, Dec. 1989.

[69] Vucetic B., Nicolas J., "Construction of M-PSK Trellis Codes and Performance Analysis over Fading Channels," *Proc. IEEE ICC '90*, pp.614-618, 1990.

[70] Monsen P., "Adaptive Equalization of the Slow Fading Channel," *IEEE Trans. Commun.*, vol.22, no.8, pp.1064-1075, Aug. 1974.

[71] Qureshi S.U.H., "Adaptive Equalization," *Proc. IEEE*, vol.73, no.9, pp.1349-1387, Sept. 1985.

[72] Monsen P., "Feedback Equalization for Fading Dispersive Channels," *IEEE Trans. Inform. Theory*, vol.17, no.1, pp.56-64, Jan. 1971.

[73] Monsen P., "Theoretical and Measured Performance of a DFE Modem on a Fading Multipath Channel," *IEEE Trans. Commun.*, vol.25, no.10, pp.1144-1153, Oct. 1977.

[74] Monsen P., "MMSE Equalization of Interference on Fading Diversity Channels," *IEEE Trans. Commun.*, vol.32, no.1, pp.5-12, Jan. 1984.

[75] Long G., Ling F., Proakis J.G., "The LMS Algorithm with Delayed Coefficient Adaptation," *IEEE Trans. Acoust., Speech, Signal Processing*, vol.37, no.9, pp.1397-1405, Sept. 1989.

[76] Eyuboğlu M.V., "Detection of Coded Modulation Signals on Linear Severely Distorted Channels Using Decision-Feedback Noise Prediction with Interleaving," *IEEE Trans. Commun.*, vol.36, no.4, pp.401-409, April 1988.

[77] Zhou K., Proakis J.G., Ling F., "Decision-Feedback Equalization of Time-Dispersive Channels with Coded Modulation," *IEEE Trans. Commun.*, vol.38, no.1, pp.18-24, Jan. 1990.

[78] Eyuboğlu M.V., Qureshi S.U.H., "Reduced-State Sequence Estimation with Set Partitioning and Decision Feedback," *IEEE Trans. Commun.*, vol.36, no.1, pp.13-20, Jan. 1988.

[79] Eyuboğlu M.V., Qureshi S.U.H., "Reduced-State Sequence Estimation for Coded Modulation on Intersymbol Interference Channels," *IEEE J. Selec. Areas Commun.*, vol.7, no.6, pp.989-995, Aug. 1989.

[80] Duel-Hallen A., Heegard C., "Delayed Decision-Feedback Sequence Estimation," *IEEE Trans. Commun.*, vol.37, no.5, pp.428-436, May 1989.

[81] Chevillat P.R., Eleftheriou E., "Decoding of Trellis-Encoded Signals in the Presence of Intersymbol Interference and Noise," *IEEE Trans. Commun.*, vol.37, no.7, pp.669-676, July 1989.

[82] *BOSS User's Manual for Version 2.0.1*, COMDISCO Systems, Inc., 1989.

[83] Sachs L., *Applied Statistics - A Handbook of Techniques*, Springer-Verlag, 1984.

[84] Paiement R.V., Chouinard J.-Y., "Simulated Application of Trellis Coded Modulation to the Indoor Wireless Channel," to be presented at the 41st *IEEE Veh. Technol. Conf. '91*, May 1991.